Earth and Planetary Sciences ETDs   Electronic Theses and Dissertations

Spring 4-17-2017

Classifying microseismicty at Mount St. Helens using a large-N array

Margaret E. Glasgow
University of new mexico

Follow this and additional works at: https://digitalrepository.unm.edu/eps_etds

Part of the Geology Commons, Geophysics and Seismology Commons, Other Earth Sciences Commons, and the Volcanology Commons

Margaret Elizabeth Glasgow
Candidate

Earth and Planetary Sciences
Department

This thesis is approved, and it is acceptable in quality and form for publication:

Approved by the Thesis Committee:

Dr. Brandon Schmandt , Chairperson

Dr. Tobias Fischer

Dr. Steven Hansen

Dr. Mousumi Roy

CLASSIFYING MICROSEISMICITY AT MOUNT ST. HELENS USING A LARGE-N ARRAY

by

MARGARET ELIZABETH GLASGOW

**B.S. GEOLOGY,
UNIVERSITY OF NORTH CAROLINA WILMINGTON**

THESIS

Submitted in Partial Fulfillment of the
Requirements for the Degree of

**Master of Science
Earth and Planetary Sciences**

The University of New Mexico
Albuquerque, New Mexico

May 2017

Classifying microseismicty at Mount St. Helens using a large-N array

by

Margaret Elizabeth Glasgow

B.S., Geology, University of North Carolina Wilmington, 2014

M.S., Earth and Planetary Sciences, University of New Mexico, 2017

ABSTRACT

A dense array of ~1,000 continuously recording, short-period geophones was deployed in the summer of 2014 within ~15 km of Mount St. Helens. Two earthquake catalogs created using reverse time imaging and template detection techniques, increase the detection rate and completeness of the earthquake catalog when compared to the permanent network, Pacific Northwest Seismic Network, catalog. An investigation into event type for ~200 of the earthquake detections leads to the discrimination of two major classification groups, volcano-tectonic and long period. Previous to this study, long period earthquakes had not been identified in the upper crust during a volcanically inactive period and our results lead us to believe they are detected but routinely misidentified as surface-generated signals and consequently, removed from the Pacific Northwest Seismic Network earthquake catalog. Earthquake locations from the reverse time imaging and template detection catalogs are mainly distributed in a volume directly beneath the summit crater between 0–6 km below sea level with a width of ~1–3 km. Volcano-tectonic and long period earthquakes occur in the same source volume, suggesting multiple source processes, and have no apparent temporal relationship. Their location is of particular interest because it is between the main upper crustal magma reservoir (~5–15 km below sea level) and the

volcanic edifice (0–2.5 km above sea level), as well as directly above the location where melt last equilibrated (~5-12 km below sea level) during the 1980 eruption. Future efforts should focus on creating LP template detections to prevent their misidentification during normal monitoring periods and enable tracking the occurrence of LP seismicity through time. Additionally, dense three-component recordings will be necessary to constrain the source mechanism of the upper crustal LP earthquakes and potential relationships to magmatic processes.

TABLE OF CONTENTS

LIST OF FIGURES

1. INTRODUCTION

Volcanic settings are a challenging field area for earthquake seismology due to the variety of potential source mechanisms including tectonic, magmatic, hydrothermal, and surficial processes. In addition, complex crustal structure creates strong path effects that distort the various source signals. Current seismic monitoring networks are generally composed of several seismometers within tens of kilometers of volcanic centers making the detection and discrimination of diverse signals difficult, especially for low magnitude (M) events. The detection threshold and ability to discriminate different source types in the presence of strong path effects could be improved with denser sampling.

In this study, we test the capability of an array of nearly 1,000 rapidly deployable short period seismometers that prioritize spatial sampling over the recording bandwidth and noise-floor at each site. We seek to quantitatively classify the diversity of recorded seismic source signal and estimate their locations. Volcano-tectonic (VT) earthquakes in the upper crust and deep long period earthquakes in the middle-to-lower crust are frequently recorded by the long-term networks at Mount St. Helens. The short-term availability of a dense array allows greater scrutiny of those source types as well as a systematic search for other types of sources that may evade detection by the long-term network. Regardless of previous detection, long period seismicity at any depth is of interest because the source mechanisms of these events are debated and potentially valuable as indicators of fluid migration or volume changes. Our findings include increased completeness of VT earthquake detections, and the identification of long period earthquakes at a previously unrecognized depth range during a quiescent period.

2. BACKGROUND

2.1 Mount St. Helens volcanism and seismicity

Mount St. Helens is part of the Cascade volcanic arc. Magmatism driven by the subduction of the Farallon and later the Juan de Fuca plates beneath the northwestern U.S. has occurred since ~40 Ma (Defant & Drummond, 1993), but volcanic edifices such as Mount St. Helens are more transient. The oldest volcanic products attributed to an eruptive center at the current location of Mount St. Helens are dated to ~300 ka (Clynne et al., 2008). It is notable that Mount St. Helens is located anomalously far west, ~50 km toward the forearc, compared to the main axis of the Cascade volcanic arc. As a result, the young and warm slab lies at a relatively shallow depth, ~60–65 km (McCrory et al., 2004).

Eruptions at Mount St. Helens have a range of compositions from basalt to andesite to dacite with most recent eruptions (e.g. 1980, 2005–2006) of dacitic magmas (Mullineaux and Crandell, 1981; Iverson et al., 2006). The current surface geology includes mixed dacite and basalt domes surrounded by andesite lava flows. The last major eruption was in 1980, when a highly hazardous Plinian eruption ejected ~1 km^3 of material (Christiansen and Peterson, 1981) and the most recent activity was the dacite dome-building eruption from 2004–2008 (Moran et al., 2008). A magmatic system, like Mount St. Helens, has two general states, active when occurrence of physical unrest (e.g., surface deformation, gas emissions, earthquake swarms) is punctuated by eruptions and inactive when there is no apparent physical unrest but deeper magmatic processes may still occur. Among the Cascade arc volcanoes, Mount St. Helens is the most volcanically and seismically active. The Pacific Northwest Seismic Network (PNSN) records more than 100 earthquake detections per year during volcanically inactive periods and thousands of detections per

year during active periods.

2.2 Types of earthquakes

A wide range of seismic signals has been identified at Mount St. Helens including volcanic-tectonic (VT), long period (LP), deep long period (DLP), and tremor events. Finding a temporal relationship between the volcanic state (e.g. dormancy, unrest, eruption) and accompanying seismicity is the initial link between types of seismic signals and volcanic processes. Tremor and VT earthquakes occur during both volcanically active and inactive periods (Shelly et al. 2007; Denlinger and Moran, 2014; Waite et al., 2008), as well as LP earthquakes with near-surface (<500 m below the surface) and surface hypocenters (e.g. icequakes, rockfalls, avalanches) (Matoza et al. 2015; Mills, 1991). LP earthquakes in the upper crust have only been identified during periods of volcanic unrest and often temporally coincide with precursory activity, dome growth, or eruptions (Matoza et al., 2015; Waite et al., 2008). DLP earthquakes are typically recorded during dormant states, however, the lack of detection during active periods may be due to interference from the large amount of shallow seismicity (Nichols et al., 2011).

VT earthquakes (**Fig. 1, A**) are the most commonly detected earthquake type at Mount St. Helens with hundreds of events detected daily by the PNSN during volcanically active periods when swarm behavior is present (Waite et al., 2008). They excite broad frequency bands spanning ~1–100 Hz at seismometers within ~10 km. VT events occur mostly beneath the summit crater at depths shallower than 5 km below sea level (bsl) and no deeper than ~10 km bsl. A map and cross section of VT earthquake locations within 6 km of the summit crater from 2009–2014 (inactive period) can be seen in **Figure 2, A-B**.

Moment tensors are rarely estimated for the VT earthquakes, making their role in the

context of magmatic processes unclear (McNutt, 2005). However, a double couple process
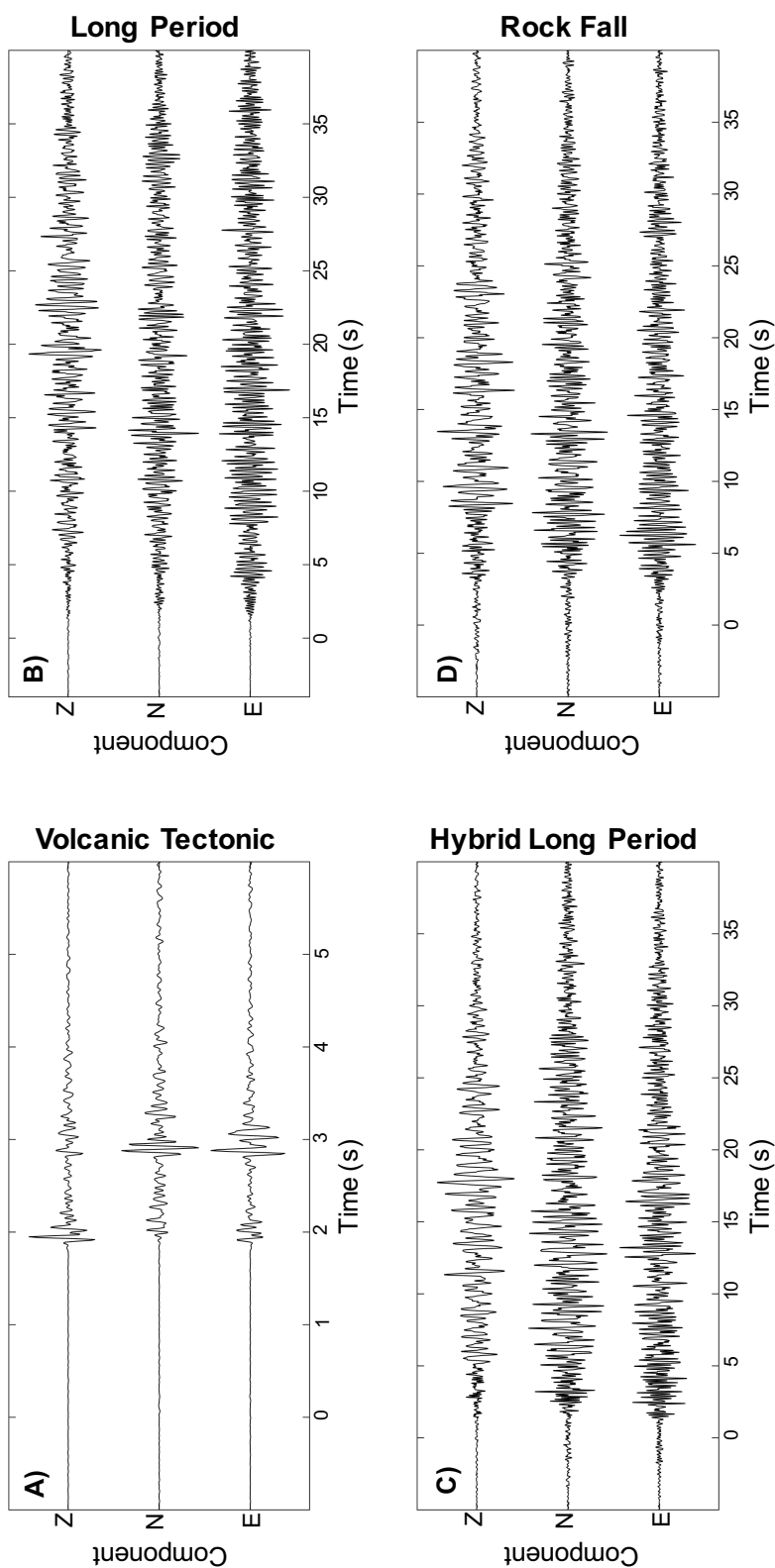

Figure 1. (A-D) Seismic signals recorded at borehole station, B202, ~6 km from earthquake locations. Time zero is estimated origin time. **(A)** 5–20 Hz waveforms for VT earthquake. **(B)** 1–10 Hz waveforms for LP earthquake. **(C)** 1–10 Hz waveforms for hybrid LP earthquake. **(D)** 1–10 Hz waveforms for rock fall event.
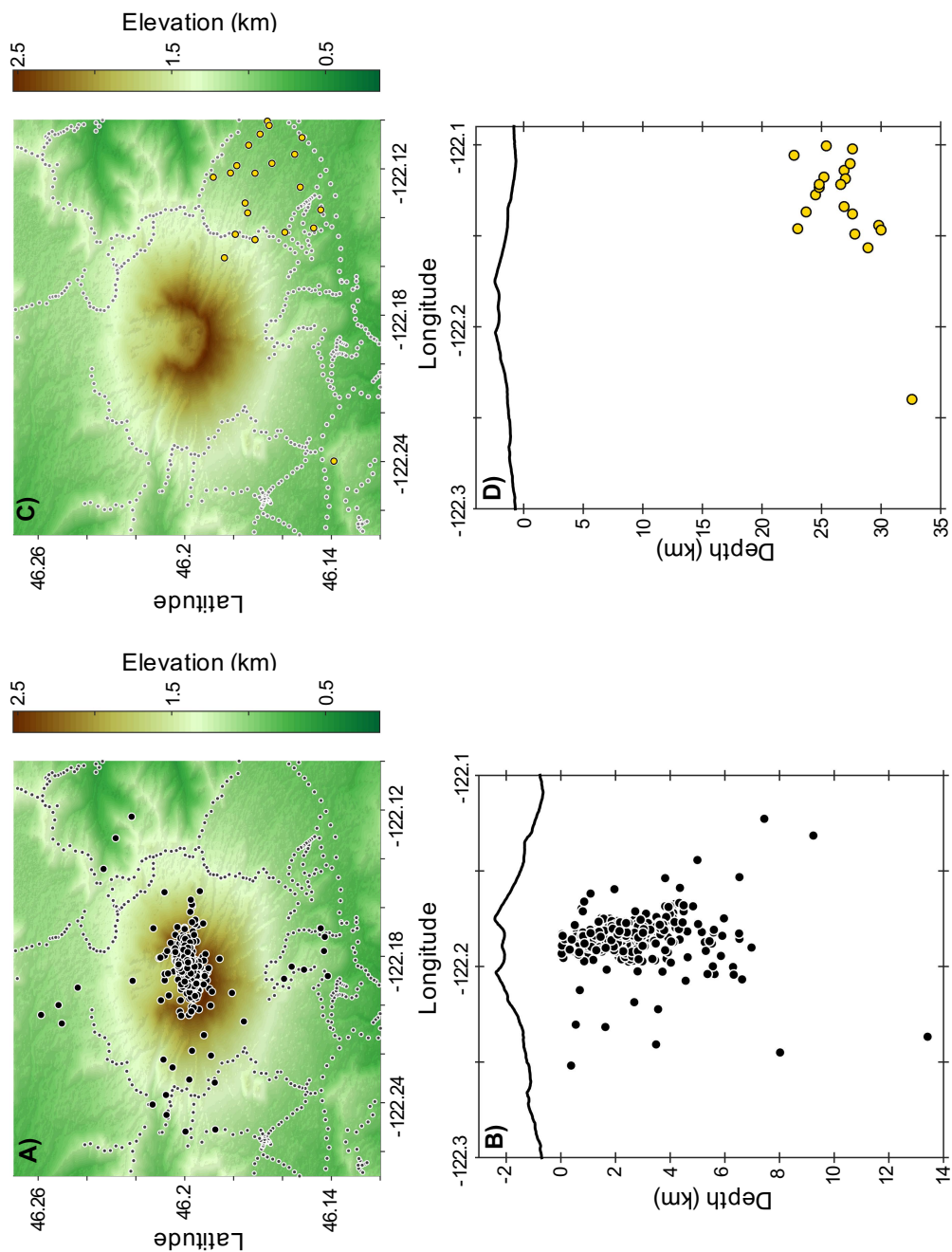
Figure 2. (A-D) Mount St. Helens earthquake locations from PNSN detections. (**A-B**) VT earthquake locations (black) from 2009–2014. (**C-D**) DLP earthquake locations (yellow) from 1970–2016.

resulting in shear failure, like dike emplacement, has been proposed as the source mechanism for VT swarm behavior in cases where focal mechanisms have been estimated (Roman and Cashman, 2006). Numerical models suggest dike emplacement involves both dike propagation (Ukawa and Tsukahara, 1996) and dike inflation (Roman, 2005), however, these mechanisms have not been clearly identified together during this process

at Mount St. Helens. The VT seismicity during an active period at Mount St. Helens, as well as the majority of arc volcanos, is most strongly attributed to dike inflation because the pressure axes are approximately orthogonal to local compressive stress (Roman and Cashman, 2006). At a number of volcanos, including Mount St. Helens, a strong temporal correlation has been observed between the horizontal rotation of fault-plane solutions and magmatic activity (Roman and Cashman, 2006). Therefore, VT earthquakes are important reflectors of a volcano's changing stress field and with continued research, possibly useful in forecasting volcanic behavior.

LP earthquakes, unlike VT earthquakes, are depleted in high frequency energy (relative to their magnitudes) and commonly associated with source processes directly involving fluids making them a distinct category of earthquake. They have a wide variety of characteristics that motivate the classification of LP seismicity in subgroups based on frequency content, hypocenter depth, and duration. At Mount St. Helens, LP earthquakes occur from the surface to ~40 km bsl, which is near the Moho (Hansen et al., 2016), but the depth distribution is not uniform (Nichols et al., 2011; Denlinger and Moran, 2014). In comparison to VT earthquakes, LP earthquakes typically have longer durations, are depleted in high frequencies, and have more emergent onsets (**Fig. 1, B**). Hybrid earthquakes combine characteristics from both LP and VT earthquakes starting with an impulsive, high frequency arrival evolving into a low frequency, long coda duration earthquake **(Fig. 1, C)** (Neuberg et. al., 2006). Tremor is a low frequency signal that lasts from minutes to months and is more commonly associated with volcanic activity but has also been observed during inactive periods at Mount St. Helens (Denlinger and Moran, 2014). DLPs most commonly occur ~5−10 km southeast of Mount St. Helens at depths

between ~20–40 km bsl and typically produce signal frequencies ≤5 Hz (Nichols et al., 2011). **Figure 2 C-D**, display the location of DLPs since 1970 by the PNSN. DLPs often occur near active volcanos, and the Cascade and Japan arcs are among the best constrained areas of DLP seismicity. They do not exhibit a clear temporal correlation with eruptions at Mount St. Helens but are suggested to indicate transport of magmatic fluids or cooling of intrusions in the mid to lower crust (Nichols et al., 2011; Aso and Tsai, 2014).

Upper crustal LP earthquakes have coda durations from ~20–50 s and peak power at frequencies between 5–15 Hz. At Mount St. Helens, they have only been observed during volcanically active periods and eruptions are often preceded by an increase in LP occurrence. In the months prior to the 1980 eruption, upper crustal LP and tremor activity occurred as magma degassed at shallow depths (~<2–3 km km below the surface) and correlated temporally with episodic edifice deformation (Scandone & Malone, 1985). The dome-building 2004–2008 eruption at Mount St. Helens was characterized by millions of LP signals, including LP drumbeating occurring every several minutes (Waite et al., 2008) and non-cyclic, near-continuous LP microseismicity (Matoza et al, 2015). In this manuscript, we refer to the LP microseismic events observed in the Matoza 2015 study, and all LP seismicity with depths <1 km, as near-surface LP events. Near-surface LP events at Mount St. Helens are often undetected due to their low signal to noise ratio (SNR). Their suggested source during the 2004–2008 eruption is a volumetrically oscillating shallow (~30 m) crack and the mechanism may be related to a pressure step and the sudden condensation of steam (Matoza et al., 2015). Although many hypotheses have been proposed, the source of LP earthquakes is still poorly understood and disagreements involve the contribution of coupling along the crack or conduit wall, the geometry of the

crack or conduit, or other sources of mechanical energy (McNutt, 2005).

In seismology, surface-generated signals are often poorly constrained as a seismic source, especially at volcanos. Icequakes, and mass wasting events such as rockfalls and avalanches occur at Mount St. Helens and produce LP signals with characteristic low frequencies and long durations **(Fig. 1, D)** (Moran et al., 2008). Mass wasting events occur dominantly in the summer months inside of the summit crater with a rate of about one rockfall per minute during a study period of several days in July 1989 (Mills, 1989). Glacial seismicity is another potential surface source (e.g. Thelen et al., 2013) because a small glacier has formed in the well-shaded summit crater of Mount St. Helens.
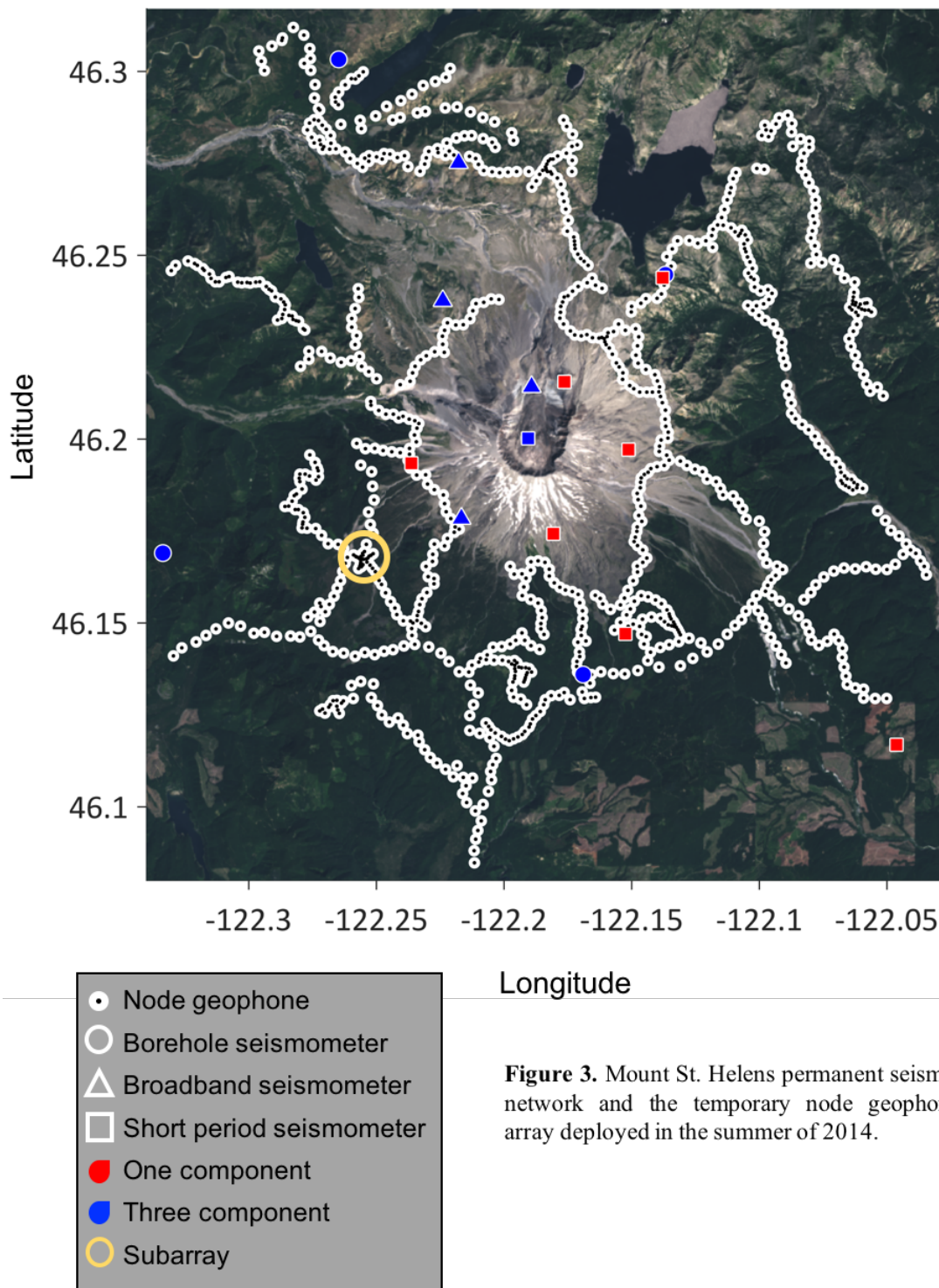
2.3 Permanent network

Monitoring efforts at Mount St. Helens have drastically increased since the 1980 eruption and recognition of the potential hazard. Prior to the 1980 eruption, there was one seismometer within a 50 km radius of the volcano. Since the eruption, monitoring has been a major priority of the PNSN with ~5 to 10 continuously recording seismometers, including one component and three component short-period, as well as three component broadband seismometers (**Fig. 3**). In 2004 an infrasound array was deployed ~13 km from the summit crater to investigate the low frequency acoustic energy produced by an active volcano (Matoza et al., 2007). In addition, the Plate Boundary Observatory (PBO) installed four borehole seismometers in 2005. With ~15 continuously recording seismometers within a 15 km radius of the summit crater, Mount St. Helens is the most seismically monitored volcano of the Cascade Range. With the intensification of monitoring since 1980, our understanding of subsurface structure and earthquake occurrence and locations at Mount

St. Helens has greatly improved. In 2014, a large four-year collaborative project, imaging Magma Under St. Helens (iMUSH; imush.org) began with the goal to geophysically image beneath Mount St. Helens from the surface to the slab interface for a better understanding of the magmatic plumbing system of an active continental arc volcano.

2.4 Geophone array deployment in 2014

Over a four-day period a dense array of 904 autonomous geophones was installed along the road and trail system within 15 kilometers of Mount St. Helens (**Fig. 3**). The 10-Hz geophones, referred to as nodes, recorded continuously at a 250 Hz sampling rate for the two-week volcanically inactive period from late July to early August 2014. The active source component of the iMUSH experiment was concurrent with the continuously recording geophone deployment. The two weeks of continuous recording coupled with the 23 active source explosions provide a unique seismic dataset from an active volcano.

The deployment of large N-array cable-free nodes has been in practice by the oil industry since ~2005 (Freed, 2008). Over the following several years, interest in this recording technology increased because of the success of node arrays in challenging field areas such as highly-populated urban areas like Long Beach, CA (Slater and Hollis, 2012). Nodes are lightweight (~5.5 lbs) and self-contained, meaning all necessary equipment (sensor, analog-to-digital converter, battery, GPS clock, memory) is within the instrument. The compact equipment and straightforward installation of the nodes decreases in-field time, making the deployment and demobilization of large node arrays more financially and logistically viable than traditional passive source networks. From a quantitative perspective, the deployment at Mount St. Helens yielded ~100 Gb of data per day resulting

Figure 3. Mount St. Helens permanent seismic network and the temporary node geophone array deployed in the summer of 2014.

in 1 Tb overall. The limiting factors of the geophones used in this experiment are the two-week battery life, the poor recording of frequencies lower than ~1 Hz, and the only vertical component instrument, which prevents three component analysis.

The dense sampling afforded by large N-arrays is particularly important in a volcanic setting. Complex shallow crustal structure due to repeated building and destroying of volcanic edifices results in highly scattered wave fields and often low signal-to-noise seismic recordings that vary greatly from station to station and are challenging to interpret given the wide range of possible seismic sources (Neuberg and Pointer, 2000; Chouet et al., 1997). Using a large N-array in a volcanic setting allows for improved detection capacity, classification of a more diverse range of signals (including VT, LP, DLP, surface signals), and increased ability to identify source processes due to better separation of high frequency source and path effects.

3. METHODS

3.1 Detection

Reverse-time imaging (RTI), within a 10 km cube centered beneath Mount St. Helens at sea level, automatically detected and located 212 earthquakes (Hansen and Schmandt, 2015). Magnitude estimates based on coda duration were also calculated for each event to maintain consistency with PNSN catalog in the summer of 2014. Following the RTI method, ~70 events were used as templates resulting in a total of ~2000 detections, including the 212 RTI events, within 15 km of the summit crater (Meng et al., 2016). Of the 2000 detections, ~1400 have sufficiently high enough signal quality for the calibration of magnitudes. The double difference method (Waldhuaser and Ellsworth, 2000) was used to estimate hypocenters for the ~2000 events (Meng et al., 2016). Over a five-year volcanically inactive period from 2009 to 2014, the permanent network (PNSN) detected and located 495 earthquakes within 6 km of the summit crater (700 earthquakes within ~20km of the summit crater). To address the detection capacity of a large-N two-week deployment compared to five years of traditional passive source permanent network monitoring, we create hypocenter distribution maps to compare the amount and spatial relationship of earthquakes between these three catalogs.

3.2 Classification

Volcanic earthquake classification depends largely on frequency content and signal duration. To determine the characteristics of each automatically detected event, a suite of basic time series analyses was applied to the node data within 6 km of the summit crater and permanent network data within ~8 km distance from the summit crater. In total ~225

one component short-period nodes, two short-period borehole seismometers, three broadband three component seismometers, three short-period one component seismometers, and one short-period three component seismometer are used. For each event, a topographic map with event location and node stations is plotted to compare relative location to other events. Permanent network and node velocity waveforms are filtered from 2 to 20 Hz and used to gauge detectability by visual inspection. A median envelope of the filtered waveforms provides information on the temporal distribution of signal amplitude, maximum amplitude, and coda duration. The power spectral density of each event is estimated using unfiltered waveforms and the median power is removed from each frequency band resulting in a spectrogram displaying power in excess of the background noise level across a 5-minute time window. We rely most heavily on the spectrogram and envelope to investigate the signal duration and frequency content leading to the classification of each event.

To automate event classification, a frequency index (FI) metric is calculated using spectrograms for stations within 6 km of Mount St. Helens. The RTI estimated origin time and event location are used with a 3-D travel time field to calculate time shifts for the event arrival to each station. After applying shifts, we take the median of the power spectral density for the inner ~225 stations. To estimate the coda duration, we take the median power from 3–30 Hz, find the maximum, and subtract the closest sample before and after the maximum where the SNR is lower than two. Events that overlap in time and events with coda magnitudes from the RTI analysis below zero are removed from this analysis. The FI metric is the logarithmic ratio of the median power between 10 and 50 Hz (P_{high}) and median power between 3 and 10 Hz (P_{low}) over an event's duration (Buurman and

West, 2010; Matoza et al., 2014).

$$FI = \log_{10} \frac{P_{high}}{P_{low}}$$

3.3 Earthquake location

Array seismology is a powerful tool used to increase the SNR of waveforms, minimize the scattering effect of ray paths, and locate the origin of the source. Plane wave propagation can be assumed when the distance between stations is small compared to the distance to the source (Rost and Thomas, 2002). At Mount St. Helens we use sub-arrays, dense clusters of geophones, with small widths (~1 km) in comparison to the distance to the source (~7–10 km). An apparent slowness vector ($\boldsymbol{u}_{hor}$) points from the center of an array to the source and reveals the inverse of apparent velocity (apparent slowness) of a wave front arriving to the array. Beamforming theoretically (Harjes and Henger, 1973; Rost and Thomas, 2002) increases the SNR ratio of the subarray (S) by approximately the square root of the number of instruments (M) times the SNR of a single array station (s):

$$S \approx \sqrt{M} s$$

The time series at the center of the array is:

$$x_{center}(t) = f(t) + n_i(t)$$

where $f(t)$ is the signal and $n_i(t)$ is the noise. In the time domain, shifts are calculated for each station relative to the subarray center for each back azimuth and slowness grid point. The time series for each station (i) with location $\boldsymbol{r}_i$ is:

$$x_i(t) = f(t - \boldsymbol{r}_i \cdot \boldsymbol{u}_{hor}) + n_i(t)$$

Prior to beamforming, we resample seismograms from 250 Hz to 100 Hz and filter from ~1–10 Hz to improve coherency across the sub-array. A back azimuth and apparent slowness grid from $0 - 360°$ and -1 to 1 s/km in the north and east directions is used for the

grid search over ~3400 combinations. The envelope of the median stack of the aligned traces $x_i(t)$ is calculated for all apparent slowness and back azimuth combinations ($\boldsymbol{u}_{hor}$) in the grid and is smoothed by a 0.2 s moving average. For each sample in time, we search through the possible slowness and back azimuth combinations for the five maximum amplitudes and we define the approximate maximum value as 50 percent weight of the maximum plus 50 percent weight of the average second through fifth maximum amplitudes. We define the beamtrace as the maximum value among all the median time-domain stacked traces at each time sample. The best combination of slowness and back azimuth results in the highest amplitude of the beamtrace following the eot. Using the optimal slowness and RTI epicenter location with a travel-time field from a 3-D velocity model (**Fig. 4**) (Waite and Moran, 2009), we estimate the depth of an event as a function of apparent P arrival slowness.
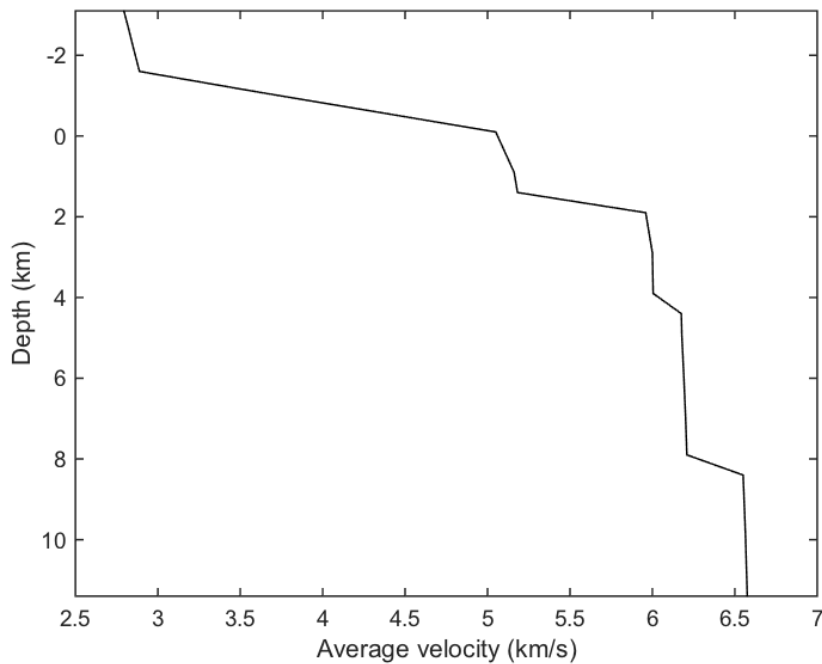

Figure 4. 1-D average P wave velocities at Mount St. Helens. Depth is relative to sea level.

To improve estimates from automated RTI locations, we also investigate absolute

locations by manually picking P arrivals, as well as S minus P arrivals when possible, from velocity waveforms filtered from 1–15 Hz. We only use the best ~20–50 node waveforms within 6 km from the summit crater for P arrival picks in addition to P, as well as S-P, picks when S arrivals are clear for three component permanent network stations. The manually picked phase arrivals are used in a grid search with 3-D travel times to find the minimum root mean square misfit corresponding to the optimal hypocenter location. The RMS misfit represents how well the earthquake hypocenter predicts the observed phase arrivals (P and S) in seconds. All measurements are weighted equally for the horizontal location. For the vertical location, we give 50% weight to S minus P picks from summit crater three component station SEP which lies directly above the majority of RTI locations and 50% weight to all other picks.

4. RESULTS

4.1 Detection

Over five years (2009–2014), 495 earthquakes are detected within 6 km of the summit crater by the PNSN. The detection capacity of the 2014 node array at Mount St. Helens resulted in approximately an order of magnitude more detections using RTI than the typical detection rate of permanent network monitoring. In a second detection effort using the node geophone data, RTI earthquakes are used as templates, resulting in another order of magnitude increase in detections, totaling ~2000 events within ~14 days. Although the number of earthquakes, detection period, and detection technique vary between catalogs, there are many spatial similarities (**Fig. 5-6**). For all three catalogs, there is one dominant zone of seismicity that is located at the center to eastern/southeastern edge of the summit crater. For the template detection catalog and five-year catalog, the 1 km^2 area of maximum concentration is the same in the latitude-longitude plane (**Fig. 5, D, F**). Also for all three catalogs, the dominant zone of seismicity is more elongated, ~3 km, in the east-west dimension and narrower, ~1.5 km, in the north-south dimension. In the longitude-depth dimension, the majority of RTI events, >70%, occur between 0 and 4km bsl (**Fig. 6, A-B**). Template detected hypocenters are predominately between 0 and 5 km bsl, slightly deeper than RTI locations and ~1 km further southeast (**Fig. 6, C-D**). There is a smaller overall geometric distribution of template detected locations in comparison to RTI locations (**Fig. 5, A, C** and **Fig 6. A, C**) but a wider area of high-density event counts. The five-year permanent network locations are tightly grouped between 0 and 4 km bsl and share a similar ~2–3 km width for the highest density event count with the template detected locations (**Fig. 6, D, F**).
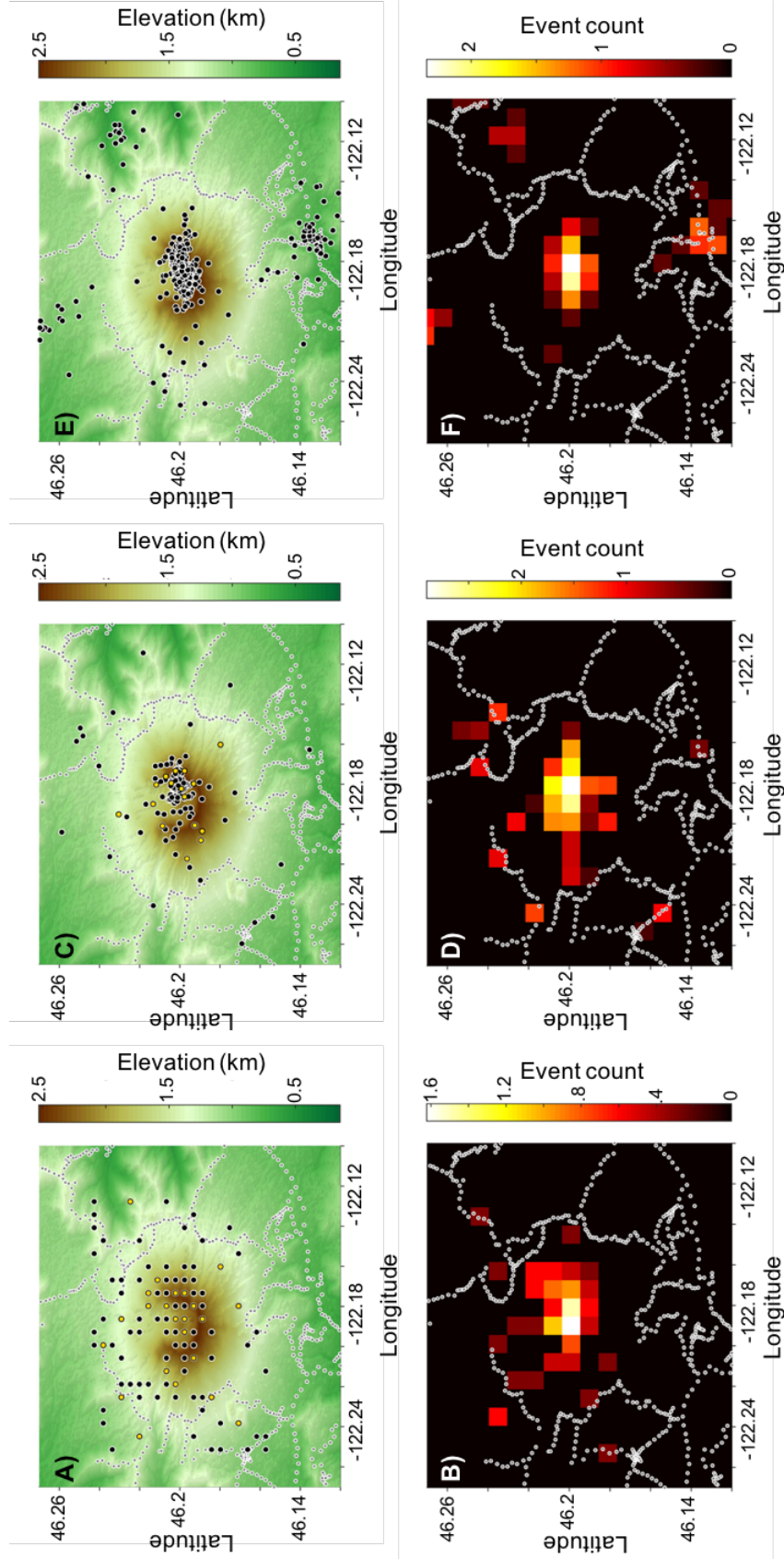
Figure 5. Mount St. Helens epicenter locations from three earthquake detection catalogs: RTI (**A, B**), template detection (**C, D**), PNSN (**E, F**). Gray and white small dots denote node locations. (**A, C, E**) Topography map with epicenter locations. Black circles are VT earthquakes. Gray and yellow circles are LP earthquakes. (**B, D, F**) Event density map with 1 km² bins over all depths. Event count is given in log scale.
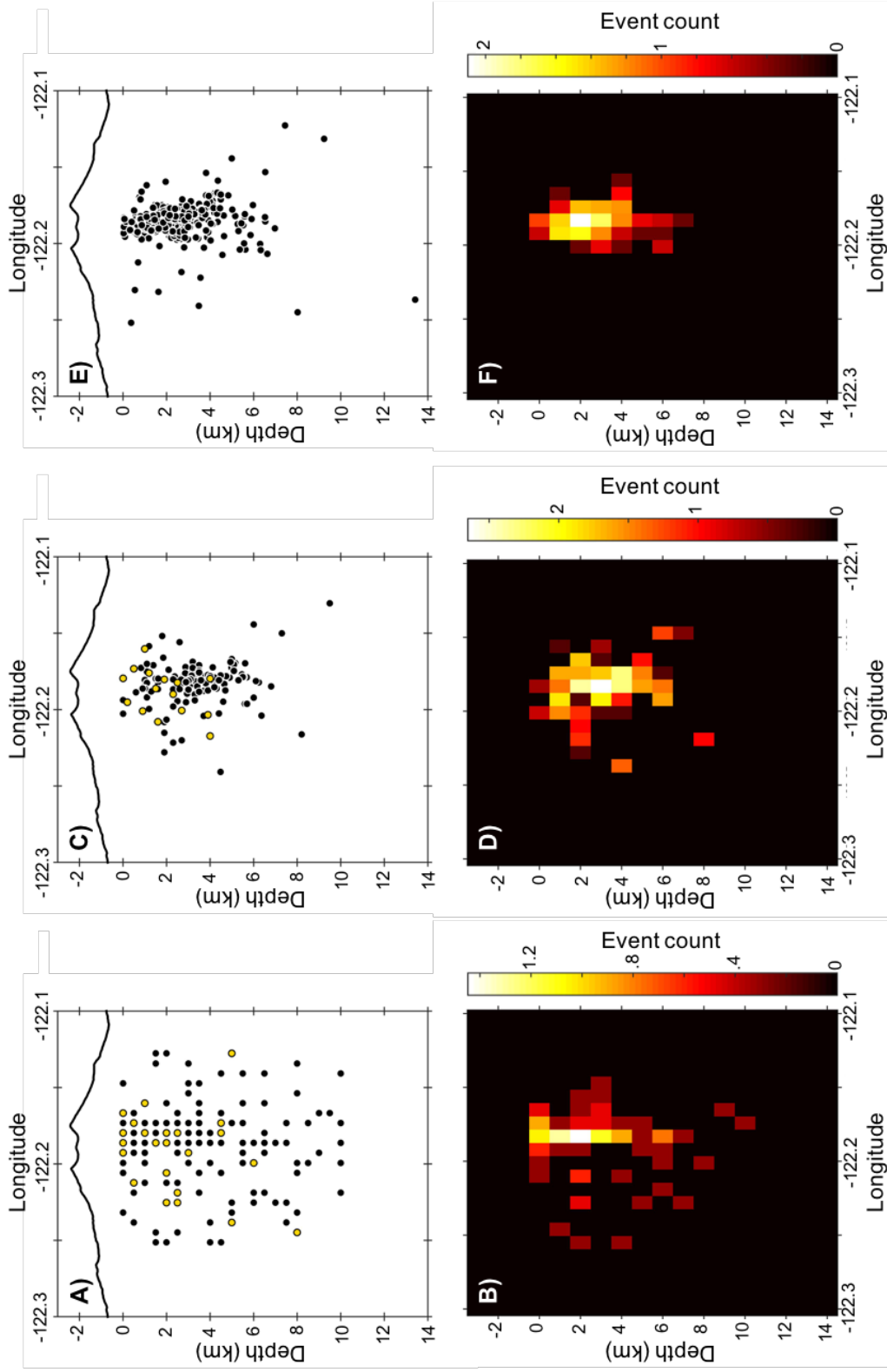
19

Figure 6. E-W trending cross section through Mount St. Helens summit crater with hypocenter locations from three earthquake detection catalogs: RTI (**A**, **B**), template detection (**C**, **D**), PNSN (**E**, **F**). Depth is relative to sea level. (**A**, **C**, **E**) Black circles are VT earthquakes and yellow circles are LP earthquakes. (**B**, **D**, **F**) Event density cross section with 1 km² bins over all depths. Event count is given in log scale.

4.2 Classification

We analyze the 212 events detected by RTI in the upper crust (<10 km bsl) and identify two distinct signal groups, VT and LP. We rely heavily on information from the spectrogram and envelope to determine event characteristics. We classify VT earthquakes by their impulsive onsets (<3 s to reach maximum envelope amplitude), short duration (<20 s), and wide frequency range (~5–100 Hz). We classify LP earthquakes by their emergent onsets (>5 s to reach maximum envelope amplitude), long duration (>20 s), and relative lack of high frequency energy with dominant frequencies less than ~10Hz. **Figure 7** displays a characteristic VT event with clean P arrivals on node and permanent network waveforms, an impulsive arrival, a short duration of ~10 s, and frequency ranging from ~3–80 Hz. **Figure 8** displays a characteristic LP event with a detectable, but less obvious P arrival on node waveforms and a barely detectable event on permanent network waveforms, an emergent arrival, a long duration of ~25 s, and lack of high frequency with the majority of power below 10 Hz.
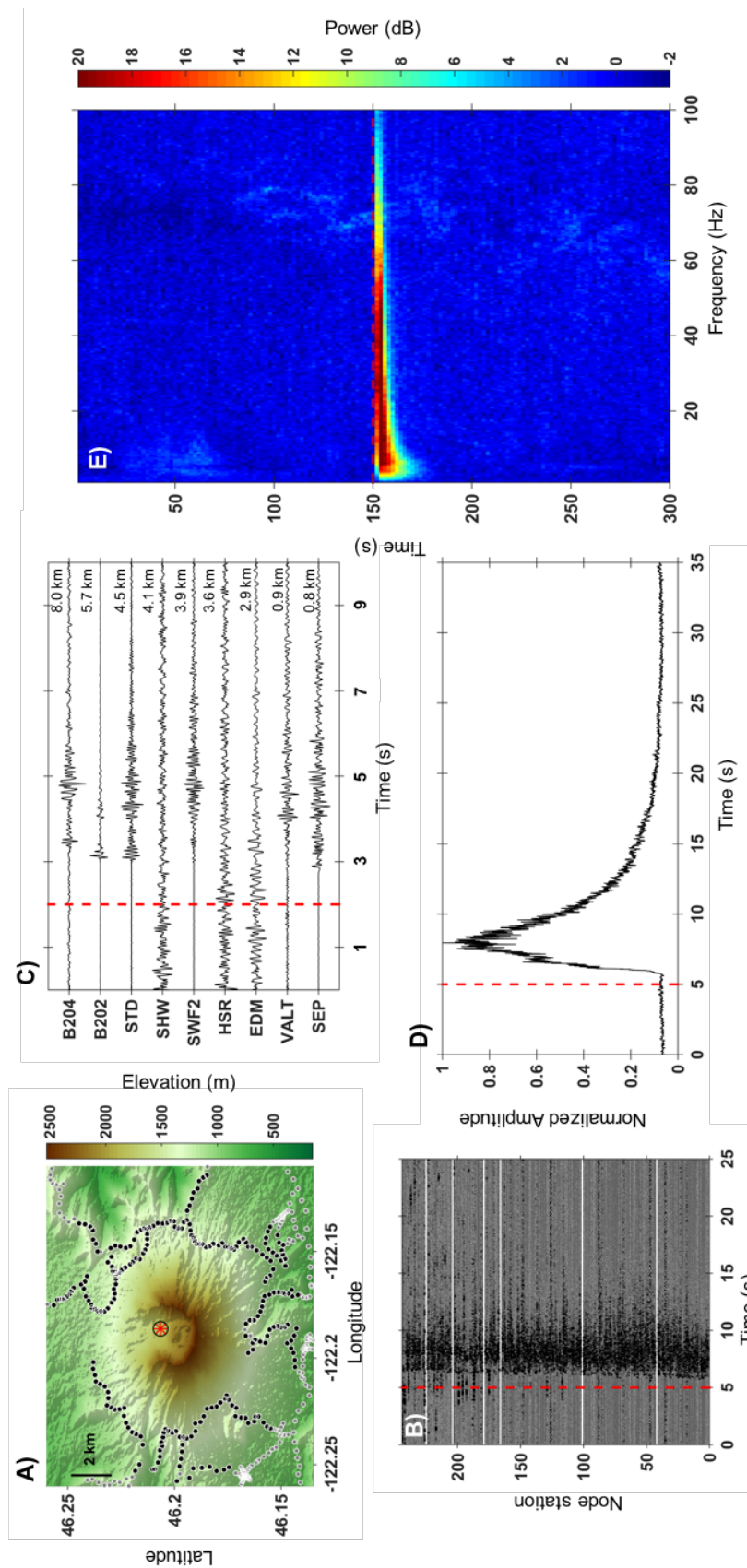
Figure 7. VT earthquake.

Figure 7 – 11. Classification of earthquakes. (**A**) Elevation map displaying RTI earthquake epicenter (red star), station locations (circles). Waveforms from stations within ~6 km of summit crater (black circles) are used to create B, D, and E. (**B**) 1–20 Hz filtered node velocity waveforms. (**C**) 1–20 Hz permanent network velocity waveforms with station names and distances relative to RTI earthquake epicenter. (**D**) Envelope of node velocity waveforms. When possible, P and S–wave arrivals are marked. (**E**) Spectrogram for node velocity waveforms displaying power in excess of median. (**B, C, D, E**) Red dashed line is RTI estimated origin time.

Figure 8. LP earthquake. See caption description Figure 6.
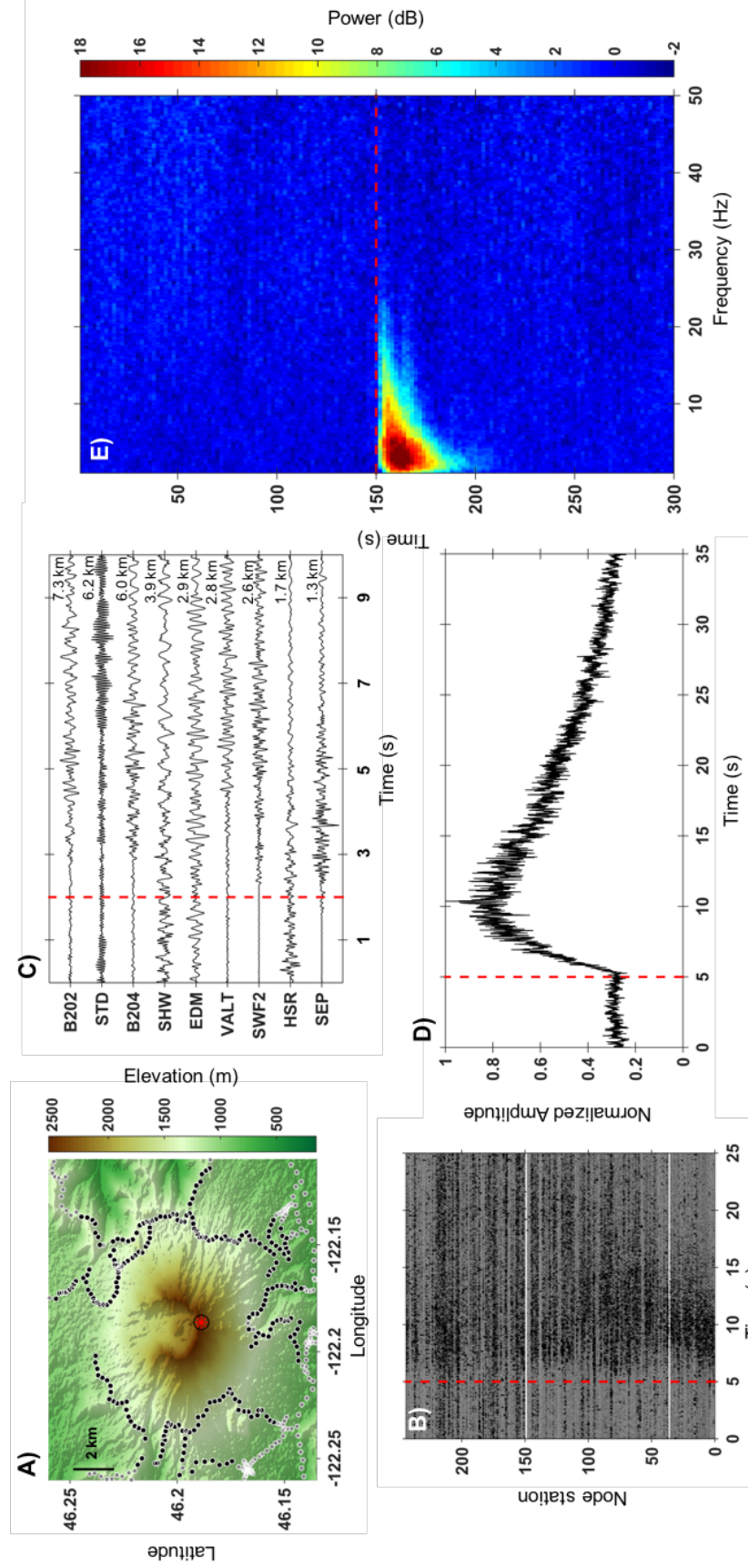
Within each group, VT and LP, we find discrepancies that allow the identification of subgroups. A subset of the regular VT earthquakes, described above, is identified as VT earthquakes with lower magnitude, and a narrower frequency band (**Fig. 9**). Compared to the VT group, the LP group is less homogenous, with variations in duration (~20–100 s), the degree that the onset is emergent, and frequency content. A subset of the LP group are hybrid LP earthquakes, still exhibiting long duration and dominantly low frequency energy but accompanied by a more impulsive and high frequency onset (**Fig. 10**). Note, the ~15–20 Hz frequency streaks with power ~4 dB are not an effect of the earthquake source and based on their frequency are likely interference from helicopters (pers. comm. Seth Moran). These two subsets are mentioned here, but for the remainder of this paper we will not distinguish them from their more generic classifications, LP and VT. Overall, ~30 events are LP and ~180 are VT, making an average occurrence of ~3 LP earthquakes per day and ~18 VT earthquakes per day during this deployment.

Additionally, we review the permanent network catalog for earthquakes occurring outside of the 10 km cube used for RTI. Two DLP earthquakes were detected during the node deployment approximately 7–8 km SW of the summit crater and at depths of 28 km and 36 km bsl. For the DLP earthquake in **figure 11**, the velocity waveforms have been filtered from 1 to 5 Hz. A clear P and S arrival at 15 and 19 s, respectively, are observed in the node velocity waveforms (**Fig. 11, B**) and in the envelope stack (**Fig. 11, D**). The event frequency is between 1–5 Hz, and the event duration is short, ~15 s, in comparison to upper crustal LP earthquakes.

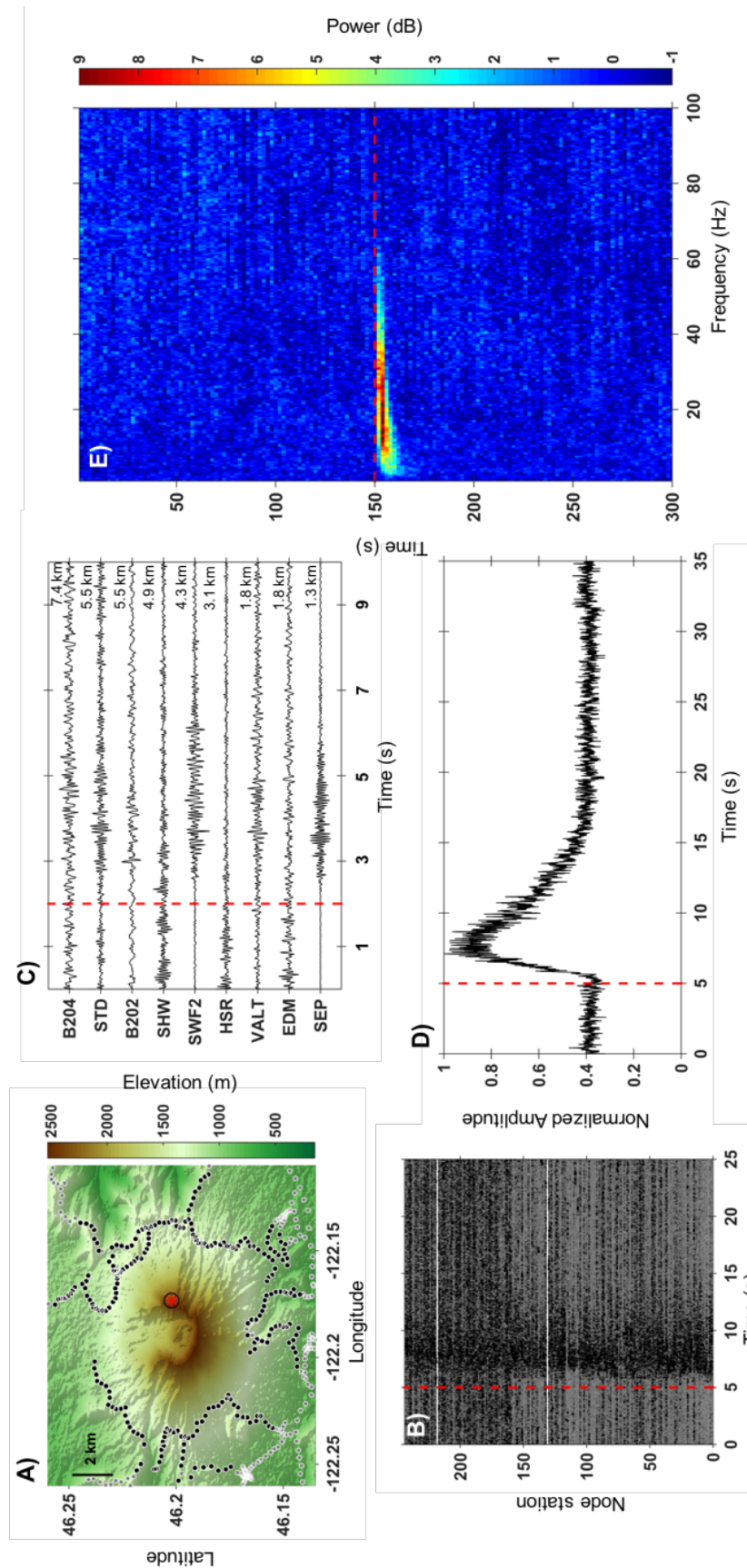**Figure 9.** Low magnitude VT earthquake. See caption description Figure 6.

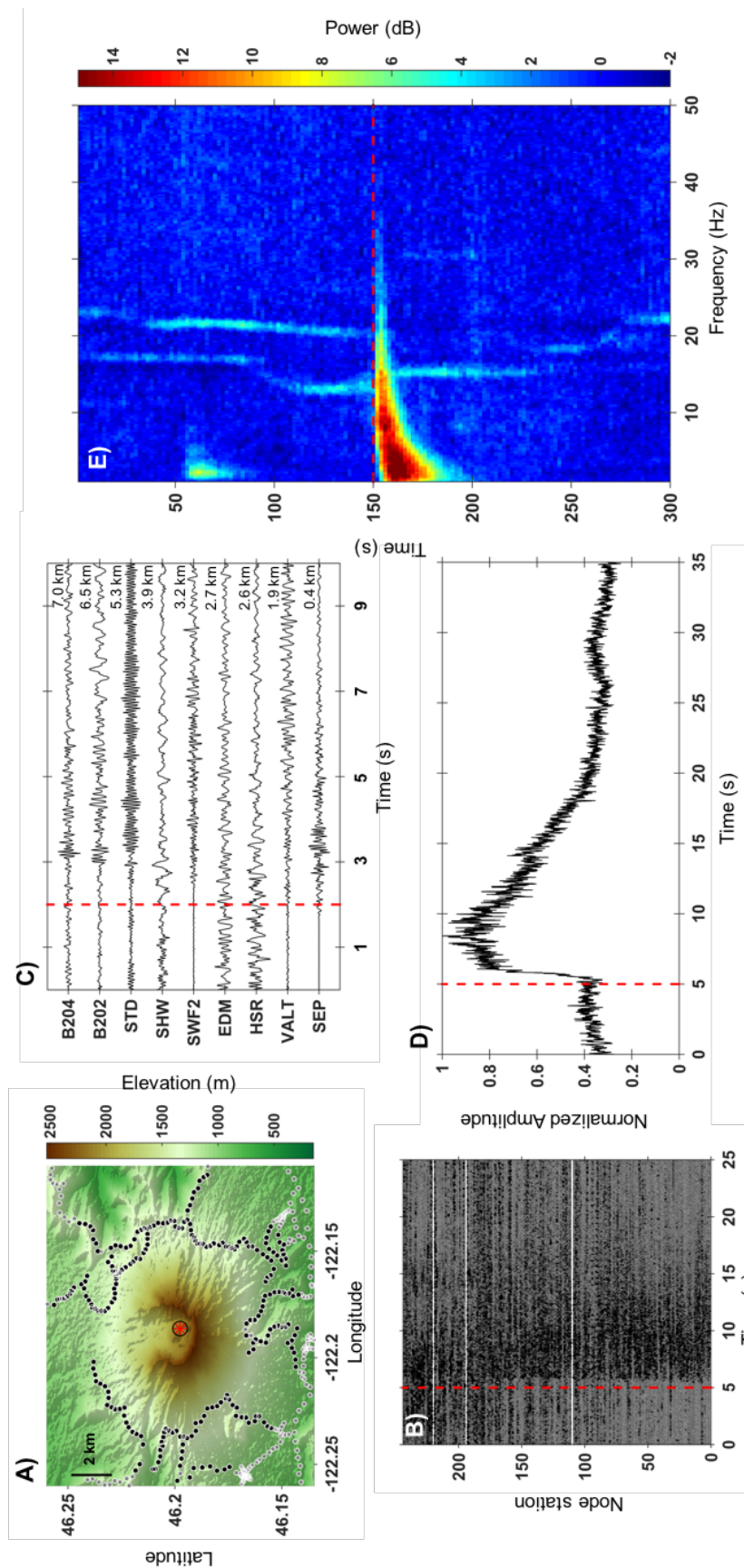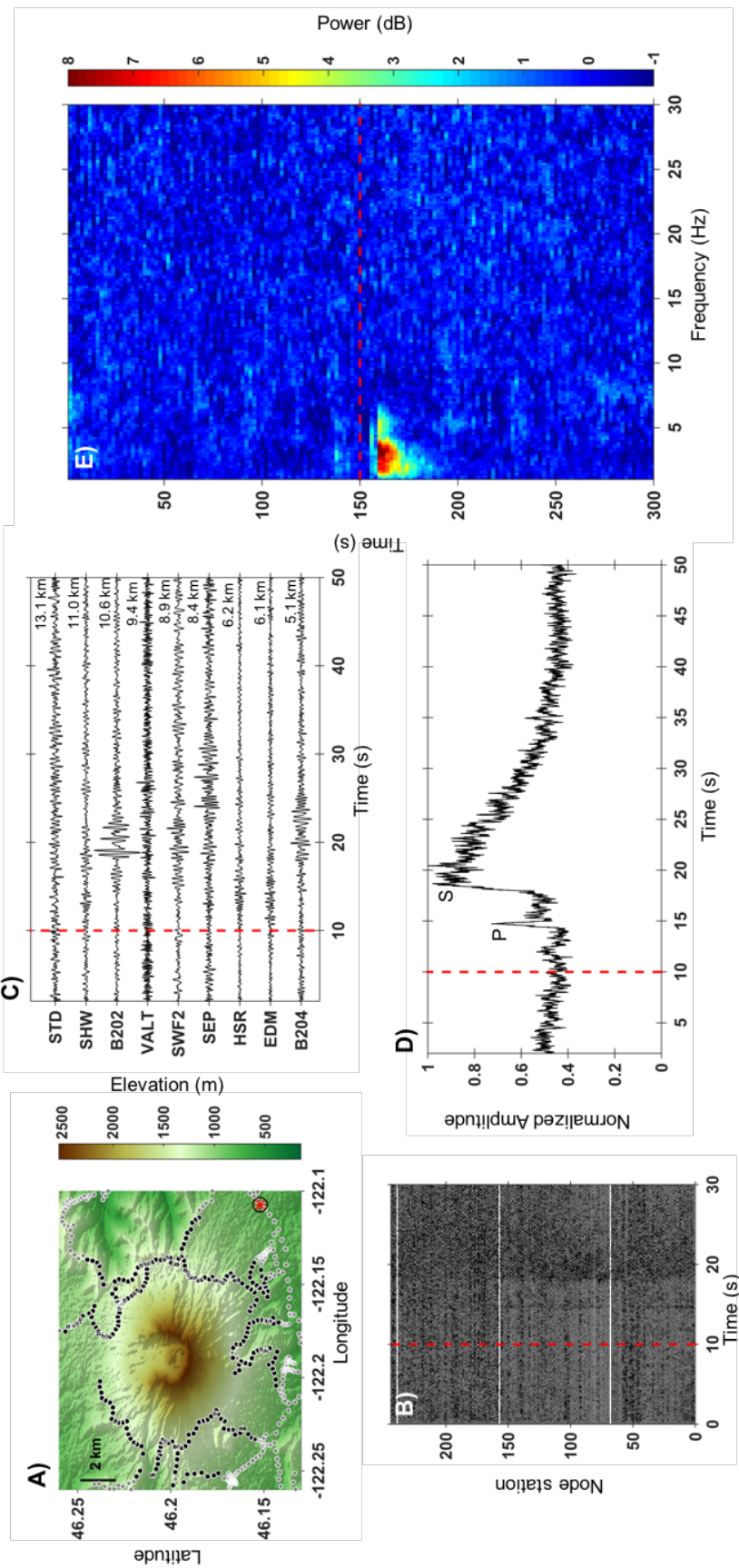**Figure 10.** Hybrid LP earthquake. See caption description Figure 6.

Figure 11. DLP earthquake. See caption description Figure 6 and note (**B**, **C**) waveforms are filtered from 1–5 Hz.

The FI metric for all events results in a spread of values from ~0 to -1 with a predominant peak at 0 (**Fig. 12, A**). By combining the FI metric and duration (**Fig. 12, B**), we systematically classify LP events as having FI ≤ -0.5 and duration ≥ 20 s. The remainder of events, FI > -0.5 or duration < 20 s, are VT. VT events have a narrower range for FI values and duration, >95% occur within a range of ~0.6 and ~25 s, respectively. Whereas, greater than 90% of the LP events occur within an FI and duration range of ~1.1 and ~40 s demonstrating higher variability of LP events when compared to VT events. This classification technique results in 105 VT signals and 22 LP signals. Their temporal and spatial relationship can be seen in **figure 12 C-D**. Of the ~30 LP signals classified through the visual analysis technique discussed previously, 19 are classified as LP using FI and duration. This discrepancy is partially due to the automation of duration, the automated removal of events that occur within 5 minutes of one another, and the lack of consideration of emergent arrivals as a classification attribute in the FI metric.

4.3 Earthquake location

A concern in the robust identification of upper crustal LP earthquakes is the ability to discriminate between LP surface and subsurface generated signals. We use beamforming analysis for the ~30 LP signals classified by visual inspection to evaluate if the wave front orientations are consistent with surface sources. In **figure 13**, LP signals are analyzed using beamforming with a subarray southwest of the summit crater (**Fig. 4**). We show two LP events with back azimuths, ~5–15° (**Fig. 13, B, E**), pointing NE toward the summit crater and they have apparent slownesses that correlate to depths of 3.5 and 6.25 km bsl, respectively (**Fig. 13, C, F**). Each of the depth estimates is greater than their corresponding

RTI depths, of 0.5 and 1.5 km bsl. Beamforming analysis results in the confirmation of at least 16 LP earthquakes with apparent slownesses of <0.1667 s/km, lower than that of the shallow crust >0.1667 s/km and consequently their sources must be deeper (>bsl) (**Fig. 14**). There are 11 LP earthquakes out of the 16 confirmed through beamforming that are also in the automated LP catalog (**Fig. 15**).

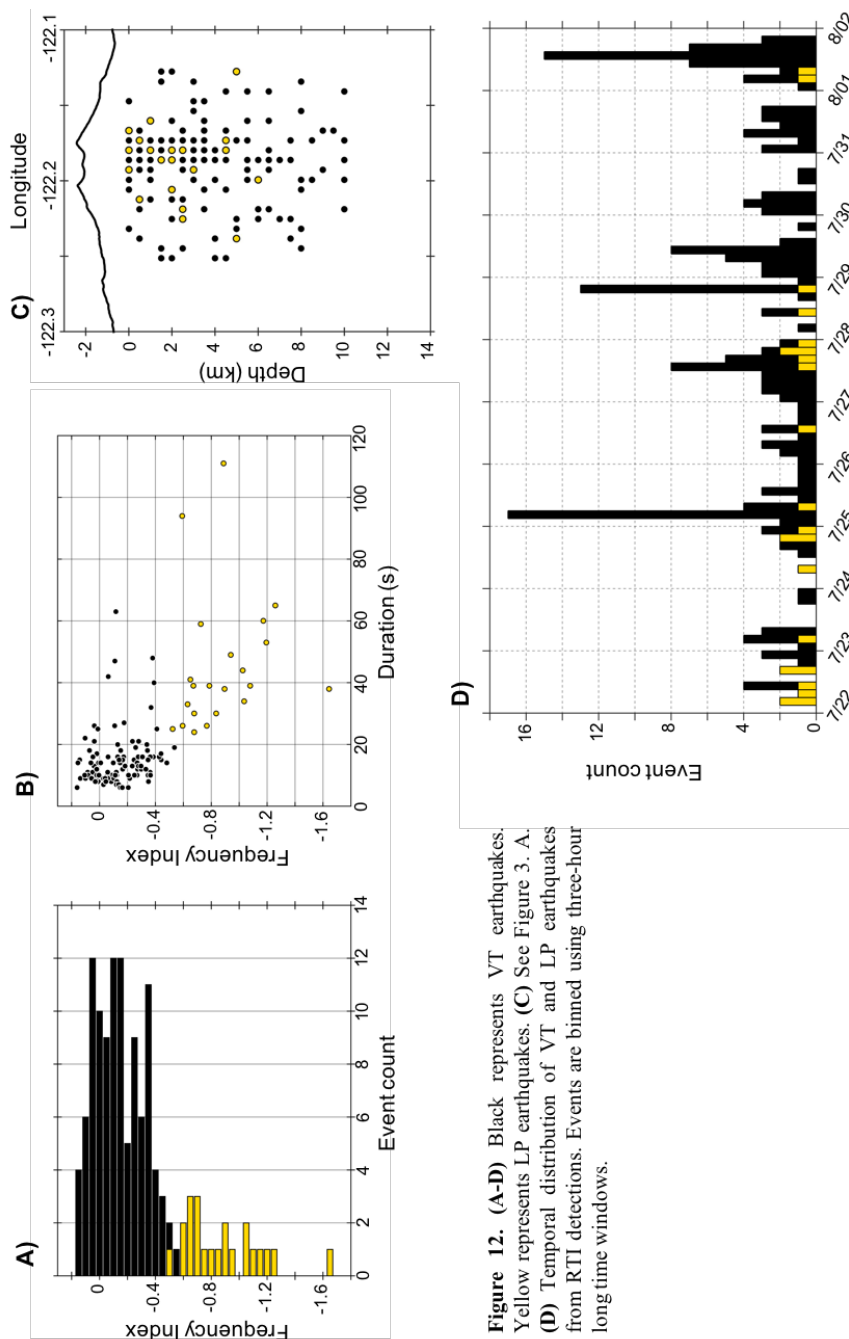
Figure 12. (A-D) Black represents VT earthquakes. Yellow represents LP earthquakes. **(C)** See Figure 3. A. **(D)** Temporal distribution of VT and LP earthquakes from RTI detections. Events are binned using three-hour long time windows.
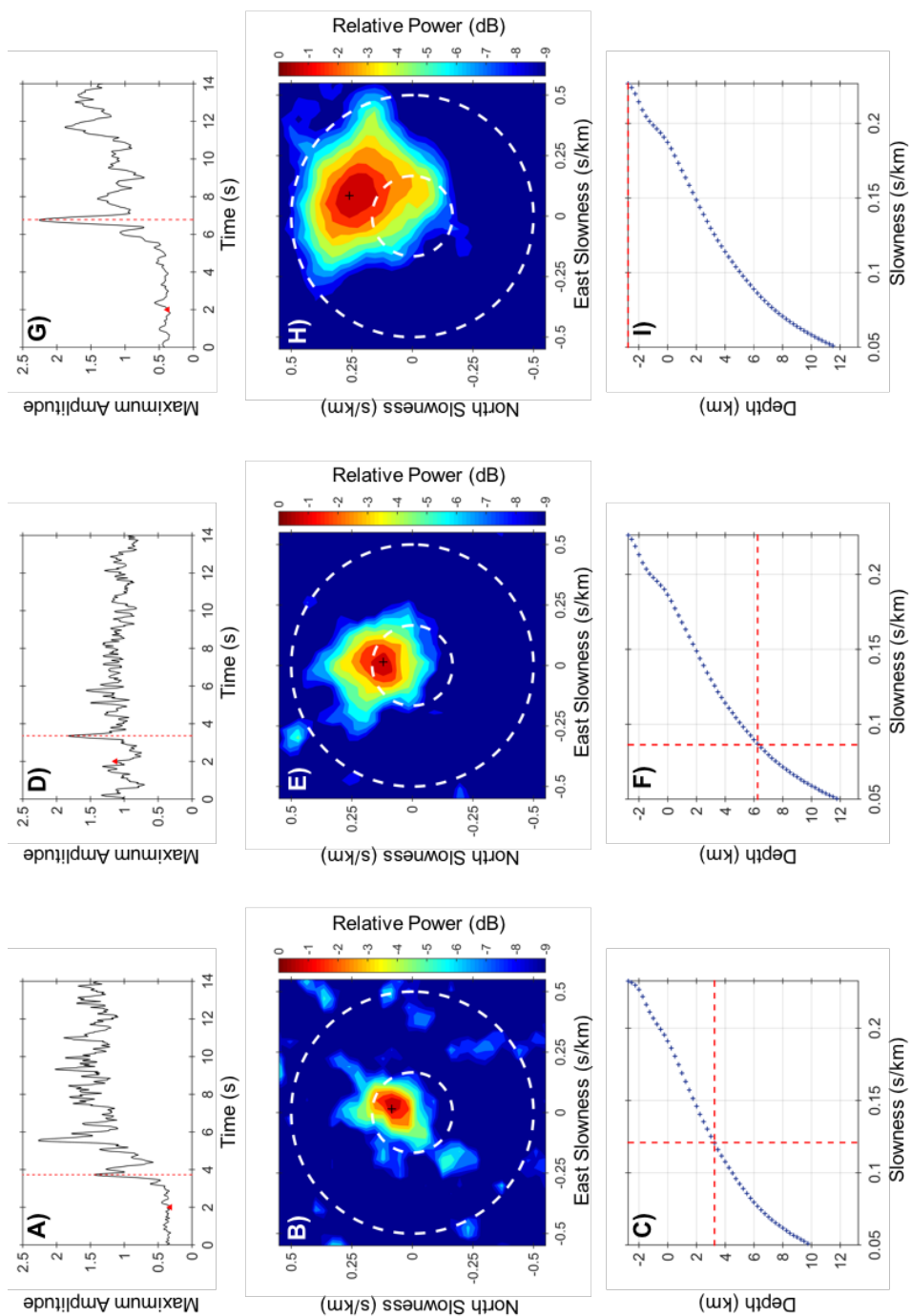
Figure 13. Beamforming analysis results for 3 LP signals: two LP earthquakes (**A-C, D-F**) and one LP surface event (**G-I**). (**A, D, G**) Maximum signal amplitude referred to as beamtrace normalized by the median. Red triangle is the RTI estimated origin time. Red dashed line represents local maxima and time sample used to make (B). (**B, E, H**) Black cross marks the strongest power which indicates the optimal apparent slowness and back azimuth. The inner and outer dashed circles represent 0.1667 s/km and 0.2 s/km, respectively. Back azimuth is clockwise and evenly spaced from 0 to 360 along circles. (**C, F, I**) Red dashed line is the corresponding depth to the optimal apparent slowness from (B). Depth is relative to sea level.
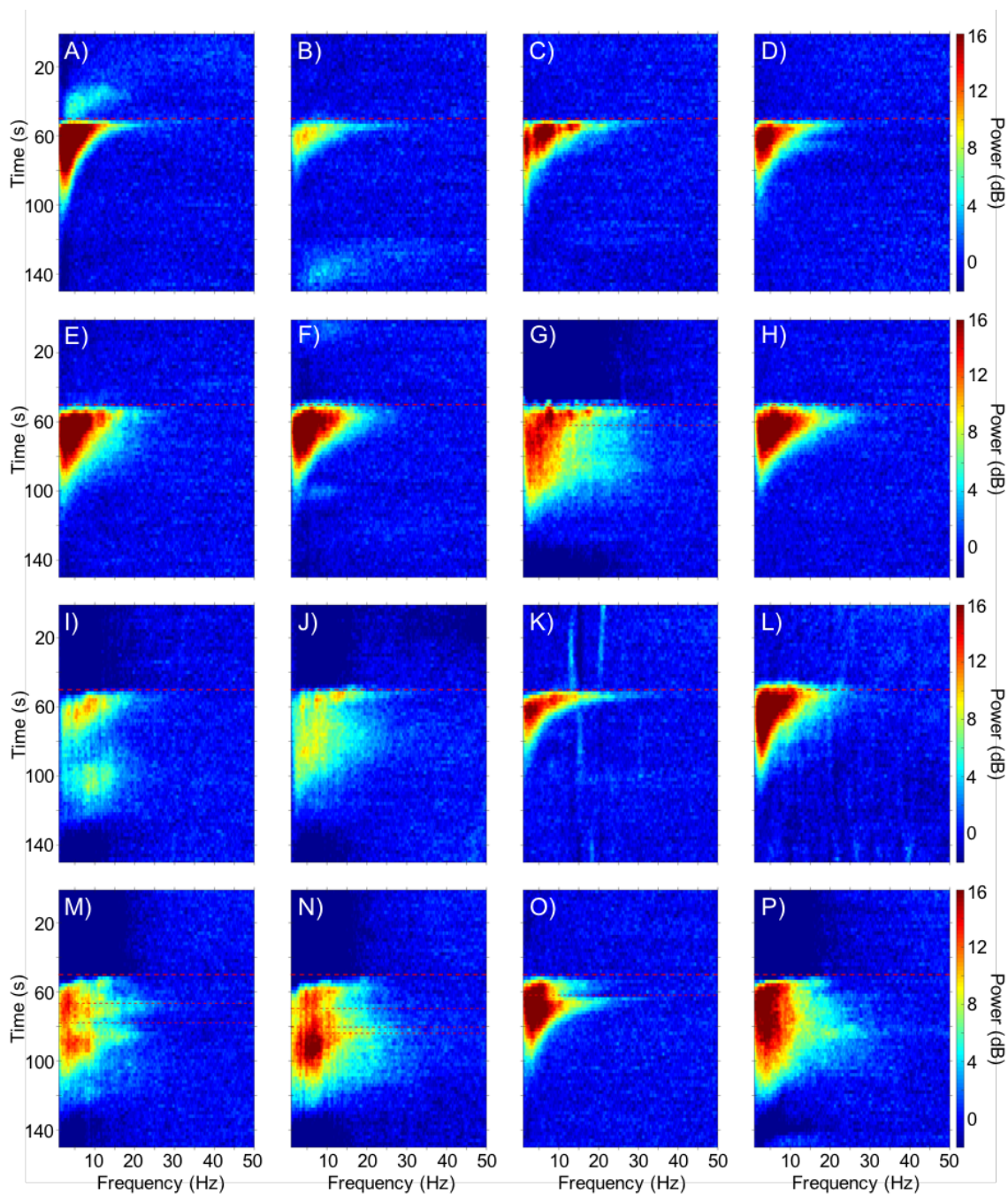
Figure 14. Spectrograms of the 16 confirmed LP earthquakes from beamforming analysis. **(A-P)** Power, frequency, and duration ranges are the same. Events are in order of occurrence. Thick, red dashed line indicates estimated origin time from RTI results. **(G, M-O)** Thin, red dashed lines indicate estimated origin time of additional events from RTI results.

Figure 15. 0.5–5 Hz waveforms for LP earthquakes recorded at borehole station, B204, ~7.5 km from epicenter locations for catalog based on visual classification (**A**) and catalog based on FI number and duration (**B**). Blue dots indicate LP earthquakes in common to both catalogs.

It is not routine for the PNSN to investigate LP signals, except DLPs, during

volcanically inactive periods because of the high number of LP surface-generated signals as well as prior to this study, upper crustal LP earthquakes were not believed to occur except during volcanically ac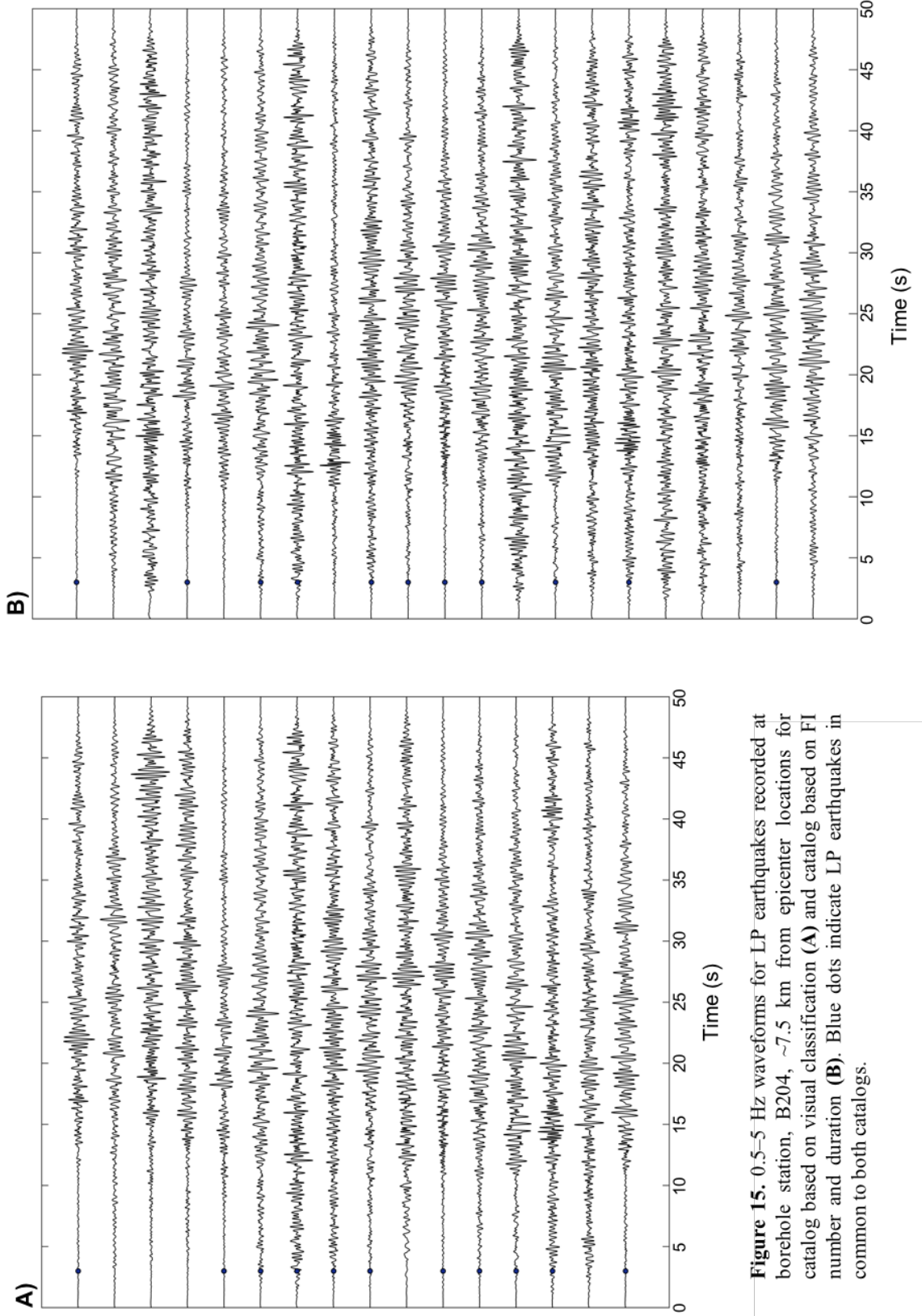tive periods. LP signals documented by the PNSN are removed from their published earthquake catalog but kept in a detection catalog that includes the estimated origin time but no location. For the approximate two-week deployment of the node array the PNSN detection catalog consists of 15 LP surface signals, which we compare to LP detection times to look for overlapping events. Note, the RTI catalog does not include LP detections above sea level (~1–2.5 km beneath the surface). Of the 16 upper crustal LP earthquakes from the RTI catalog, 8 are also found in the PNSN LP detection catalog. We assume the remaining 7 PNSN LP sources are in the suburface above sea level or at the surface and we use beamforming analysis to constrain their optimal back azimuths and optimal depths. Most of the events have very low SNRs and work poorly with beamforming but a successful example can be seen in **figure 13 G-I**, where the back azimuth of ~15° points NE toward the summit crater, the apparent slowness (~0.25 s/km) is not slow enough to be deeper than sea level and the depth as a function of slowness locates the event at the free surface of our travel time grid. Successfully locating an LP signal at the surface gives testament to the ability of our beamforming analysis at discriminating between surface and subsurface sources. We created spatial distribution maps to show the different locations and separation of the 16 confirmed upper crustal LP earthquakes and the DLP earthquakes recorded by the PNSN since 1970 (**Fig. 16, A-D)**.
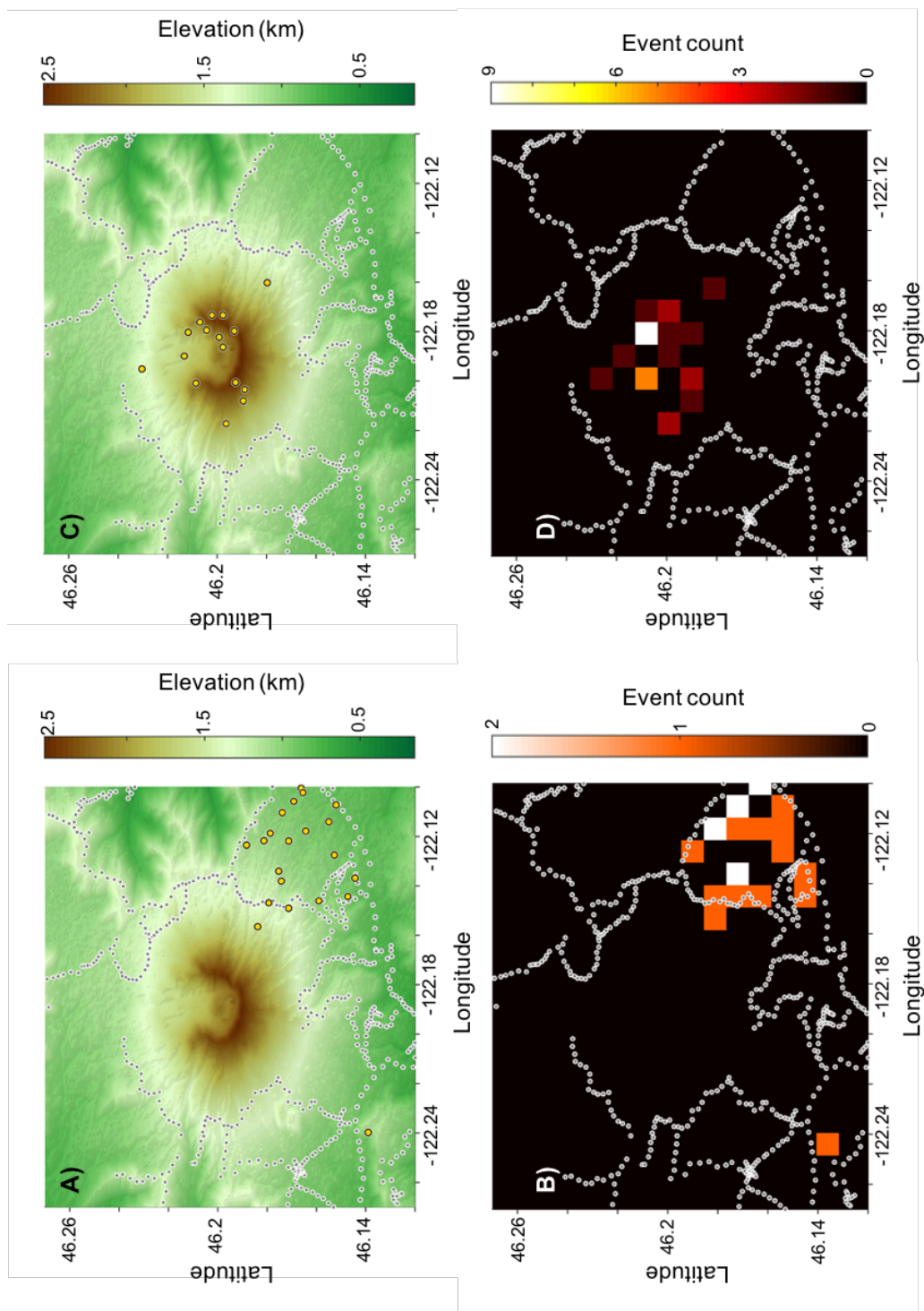
Figure 16. LP earthquake spatial distribution. Gray and white dots denote node locations. (**A, B**) DLP earthquake epicenter locations since 1970 from PNSN catalog. (**C, D**) LP earthquake epicenter locations over ten days from RTI catalog. (**A, C**) Topography map with epicenter locations (yellow dots). (**B, D**) Event density map with 1 km² bins over all depths. Event count is linear.

We estimate absolute locations for the highest signal-to-noise VT earthquakes with clear phase arrivals. The resulting hypocenter estimates are typically within the error of RTI and PNSN estimates (**Fig. 17, A-B**). Determining the absolute location of VT
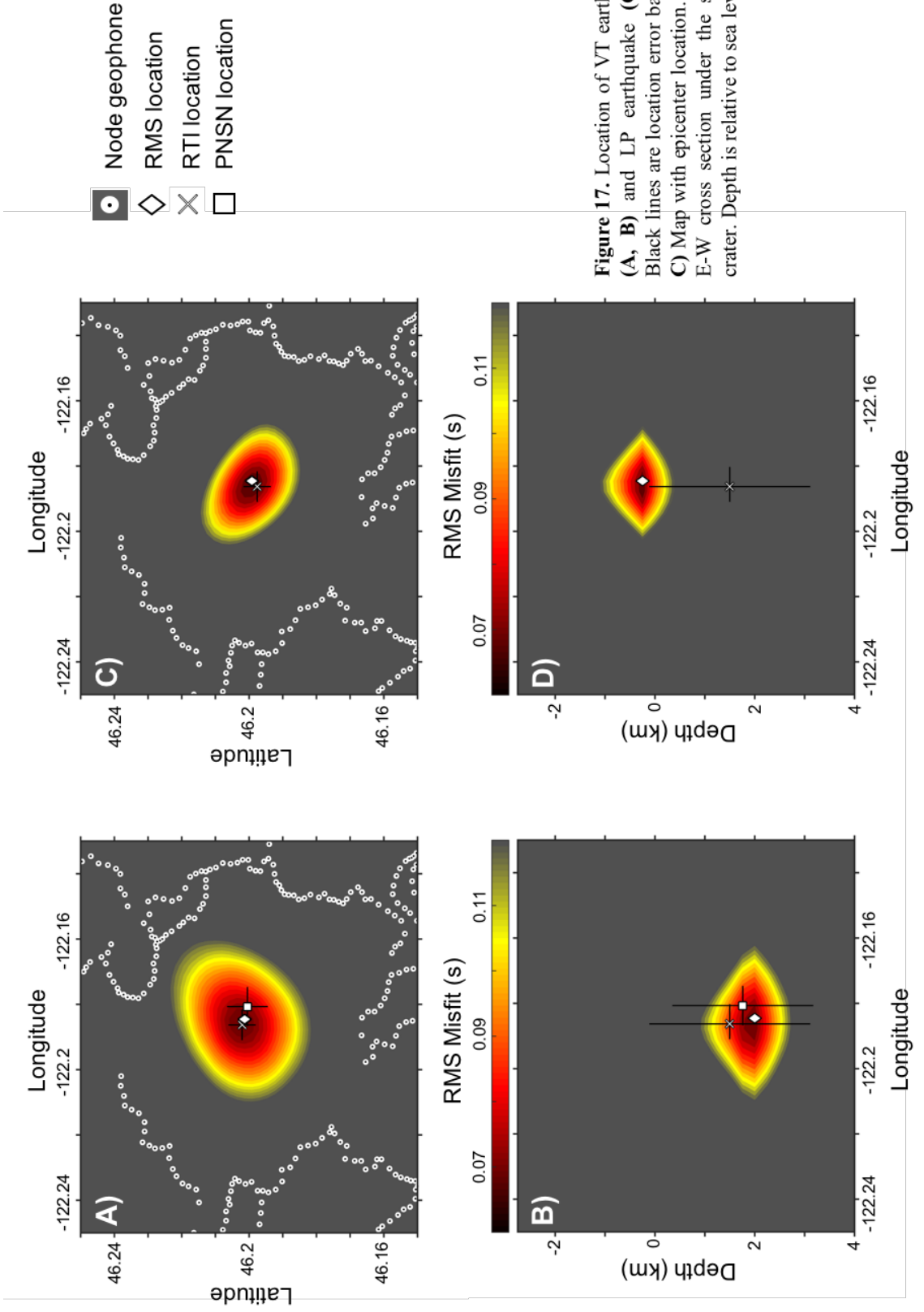
Figure 17. Location of VT earthquake (**A, B**) and LP earthquake (**C, D**). Black lines are location error bars. (**A, C**) Map with epicenter location. (**B, D**) E-W cross section under the summit crater. Depth is relative to sea level.

earthquakes is straightforward, whereas for LP earthquakes this is more difficult, with the characteristically emergent arrivals and a much smaller number of earthquakes to investigate. We can be selective in identifying ~20–50 clean velocity waveforms out of the ~900 vertical component node velocity waveforms making the horizontal locations of the 16 LP earthquakes easier to constrain than the depths. As a result, we have few 3-D locations for upper crustal LP earthquakes because most do not have clearly identifiable S arrivals on three component velocity waveforms. In **Figure 17, C-D,** the hypocenter location we estimate for the upper crustal LP earthquake agrees within error of the RTI horizontal location, and almost within error of the vertical location. Overall, our absolute depths are ~1–2 km shallower than the automated RTI location depths for upper crustal LP earthquakes. Note, there are no PNSN locations of LP signals (see previous paragraph)

5. DISCUSSION

5.1 Detection capacity

From 2009–2014, the PNSN detected on average ~1–2 earthquakes per day. During the node deployment, PNSN detections increased to an average of ~2–3 earthquakes per day. Dense spatial sampling from the node array allows for increased detections using RTI and results in an average of ~20 earthquakes per day. Template detection increases the average to ~125 earthquakes per day, this is two orders of magnitude greater than the average PNSN detection rate (**Fig. 18**). The increase in detection rate follows the Gutenberg-Richter law:

$$\log_{10}(N) = a - bM$$

where *M* is the magnitude, *N* is the number of earthquakes with magnitudes $\geq M$, and *a* and *b* are constants. The b value at Mount St. Helens ranges from 0.6–1.8 (Weimer and McNutt, 1997; Moran et al., 2008) and the RTI and template detection catalogs have b values within that range, 0.99 and 1.1, respectively (Hansen and Schmandt, 2015; Meng et al., 2016). Over the recording period, the frequency-magnitude relationship is normal for both catalogs, however, their time-frequency relationship includes several spikes in seismicity that are not present in the PNSN catalog suggesting small swarms of activity whose frequency-magnitude relationships have higher b values (**Fig. 18**). The most notable difference between the catalogs are on July 28 and from August 1–2, where the RTI and template detections have strong peaks but the PNSN records little to no detections during the concentrated activity. The node deployment at Mount St. Helens demonstrates its capacity to substantially increase the completeness of earthquake detections at an active volcano and attests to the potential usefulness of large node arrays for volcano monitoring
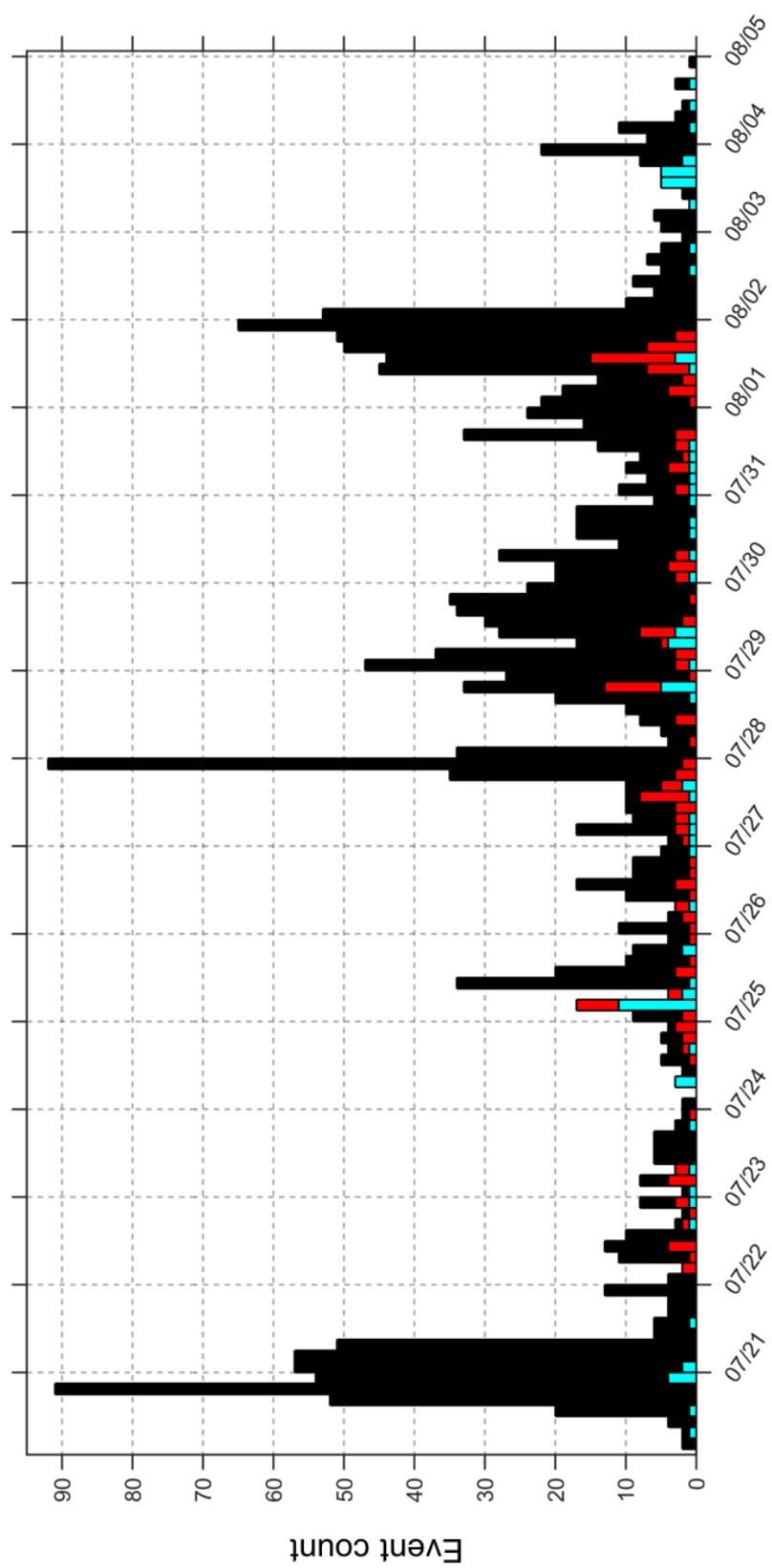
and broader volcanology research.

Figure 18. Temporal distribution of earthquakes from template detection catalog (black), RTI catalog (red) and PNSN catalog (light blue).

5.2 LP earthquakes

At MSH, surface observations (eg: hot, mineral-rich springs ~1–2 km from the summit crater) indicate hydrothermal activity in the upper few kilometers (~2 km) which is likely driven by a shallow heat source (Aizawa, et al. 2009; Bedrosian et al, 2007). Volcanic edifices are highly permeable which easily allows meteoric water to join magmatic water in the hydrothermal system. Shallow (~30 m), near-continuous, randomly occurring LP earthquakes were observed during the 2004–2008 eruption and the leading mechanism for their generation is the volumetric oscillation of a crack due to the condensation of cool meteoric water as it rapidly interacts with the warmer hydrothermal system (Matoza et al., 2015). The LP earthquakes discovered in our study are likely too deep to have the same source as the near-surface LP earthquakes, however a dilatational mechanism could be common to both.

Numerical modeling has been used to demonstrate LP signals can be produced by slow-rupture failure in unconsolidated rock (Bean et al., 2014). LP signals generated in the shallow subsurface (<1 km below the surface) as short pulses are recorded as long duration LP earthquakes at stations >~500–800 m from the epicenter. In the shallow edifice (<1 km), it is possible for VT earthquakes to morph into LP earthquakes due to weaker materials near the surface allowing for slower rupture speeds and the generation of stress-driven, rather than fluid-driven, LP seismicity (Bean, et al., 2014). The occurrence of LPs during the two-week period detected by an independent study (pers comm. Hotovec-Ellis) reveals microseismic LP earthquakes likely coming from the near-surface or surface. These earthquakes have been researched minimally but through beamforming, we confirm they are unlikely to have a depth greater than a few hundred meters. These near-surface LP

earthquakes could be due to slow-rupture in unconsolidated rock, ice-quakes, small rockfalls, or possibly meteoric water interaction with the hydrothermal system. However, the upper crustal LP seismicity we focus on in this paper is much deeper and VT earthquakes are occurring in the same area which eliminates the possibility that these LP signals result from path effects distorting VT earthquake signals. These deeper LP earthquakes are considered a different type based on their upper crustal depths and likely do not have the same source as that of near-surface LP earthquakes seen by Matoza et al. (2015) or Bean et al. (2014). When searching for potential clues related to source, upper crustal LP earthquakes can be compared to the VT earthquakes occurring during the same time period and in the same space (La Rocca and Galluzzo, 2016).

LP and VT earthquakes occur in the same source volume (**Fig. 5-6, A, C**), ~0–6 km, at Mount St. Helens during the two-week study period, suggesting at least two different processes are occurring close in time and space. The observed wide range of LP duration and frequency may suggest more than one processes is occurring or a single process with variable rates. It is also possible that LP earthquakes, such as hybrid LPs (**Fig. 10**), have a source that involves a combination of the processes producing VT and LP signals. In a recent study at Mt. Vesuvius, the source processes of VT and tremor occurring in the same source volume was investigated (La Rocca and Galluzzo, 2016).

Volcanic tremor was recently discovered at Mt. Vesuvius, a volcano that has been inactive since 1944 (La Rocca and Galluzzo, 2016). This study of inactive state, upper crustal tremor is the closest analogue we have to Mount St. Helens inactive state, upper crustal LP earthquakes. There are many parallels between analysis techniques and results from this paper and La Rocca and Galluzzo, 2016. The discovery of tremor, a type of LP

signal produced by many earthquakes in a short time, was surprising since this type of activity is associated with volcanic unrest or eruption. A seismic array, 10 stations spanning <500 m, installed in 2012 improved the earthquake detection capability at Mt. Vesuvius which led to the discovery of these low amplitude, microseismic earthquakes and beamforming was used to distinguish them from surface sources and deep sources. The tremor events are characterized by low frequency (corner frequencies from 3–6 Hz), and long duration (~60–400 s), and some tremor was recorded at distances 90 km from the volcano (La Rocca and Galluzzo, 2016). The hypocenters for the volcanic tremor, estimated by the inversion of S − P picks at three component stations combined with a velocity model, span ~5–6.5 km bsl beneath the crater. Importantly, VT earthquakes at Mt. Vesuvius span from the surface to ~6.5 km depth, meaning tremor and VT earthquakes both occur from ~5–6.5 km bsl. This is in a similar depth range but slightly deeper and more confined than the overlap of VT and LP hypocenters (0–6 km bsl) at Mount St. Helens. La Rocca and Galluzzo, 2016 hypothesize that VT earthquakes and tremor occurring in the same source volume are likely produced by the same source mechanisms because of their spectral similarities. They attributed both types to shear failure and the difference between VT and LP signals was suggested to arise from variable rupture velocity. The suggested source mechanism for tremor, in this case, is many shear failures on different fault planes in a small volume and in a short amount of time. At present, the best interpretation is that these failures occur between high viscosity (partially crystallized) magma and the surrounding conduit and produce stick-slip earthquakes. This could explain why tremor occurs on multiple fault planes with different orientations.

Although none of the LP signals were in the PNSN catalog, half of the 16 confirmed upper crustal LP earthquakes were detected by the PNSN but classified as surface generated signals and removed from their catalog. Given the diversity of LP signals (e.g. FI values, durations, and onsets) we are likely not identifying many of the diverse longer period signals produced by magmatic systems. We do not suggest all of the removed LP signals are from the subsurface but our results suggest that this type of seismicity may be systematically overlooked and potentially more common than routinely generated catalogs would suggest. This poses a problem for event classification using sparse permanent networks where beamforming techniques cannot be used. However, during normal monitoring periods template detection could be successful if subsurface LP signals have been previously identified with dense arrays. Additionally, we could increase the number of LP templates by increasing the number of RTI detections through changing the parameters to search for LP specific characteristics (e.g. frequency, duration, onset).

5.3 Possible unrest

The discovery of upper crustal LP earthquakes during a volcanically inactive state is a substantial finding in volcano seismology, which raises new questions about the level of activity beneath Mount St. Helens during the node array deployment. This period may have had higher earthquake occurrence, indicating a possible brief state of unrest (pers. comm. Seth Moran and John Vidale). The occurrence of 2 DLP earthquakes in ~10 days at Mount St. Helens is unusual and suggests at least the deeper system was experiencing an uptick in activity. The detection of VT earthquakes increased from the average ~1–2 earthquakes per day to ~2–3 earthquakes per day, however we note it is possible that PNSN

detections increased due to greater scrutiny by PNSN analysts during the large iMUSH and node experiments. During the time of the node deployment 15 LP "surface" signals were detected and of those, we have confirmed 8 were upper crustal, not surface sources. These results lead us to believe upper crustal LP earthquakes may be routinely catalogued as surface LP signals by the PNSN.

If upper crustal LP events are going undetected or being improperly classified as surface sources and there was an unusually high level of subsurface activity during the node array deployment, then we would expect increased LP detections by the PNSN during this time. There were 64 LP surface events detected by the PNSN during July and August of 2014 and 58 detected during July and August of 2015 (15 in 2013, 70 in 2012). Although there are slightly more LP signals detected in 2014, the difference is small compared to the inter-annual variability. This does not support a higher occurrence of LP seismicity, even if there was a higher occurrence of VT or DLP earthquakes. However, it is not ideal to track upper crustal LP earthquake activity by the number of events interpreted as surface sources because the fraction of false classifications is poorly constrained and many true surface sources are expected. Future studies should employ template based detection and other array processing methods to specifically identify upper crustal LP earthquakes.

A high Vp/Vs body extending from ~5–15 km bsl beneath Mount St. Helens suggests the presence of melt directly below the location of VT and LP earthquakes, ~0–6 km bsl, during the node experiment (Kiser et al., 2016). VT and LP earthquake locations are also predominately above the location that melt last equilibrated, ~5 km bsl, during the 1980 eruption (Rutherford and Hill, 1993). Tracking the occurrence of seismicity, specifically the upper crustal LP sources which may be related to fluid movement, through

time may offer a new perspective on temporal variations in magmatic activity in the depth

range between the main upper crustal magma reservoir and the summit crater.

6. CONCLUSION

An increased earthquake detection rate by two orders of magnitude and the discovery of a new earthquake during a volcanically inactive period are some of the results made possible with nearly 1000 rapidly deployable geophones within a ~15 km radial distance of Mount St. Helens. The increased detection rate led to increased completeness of the earthquake catalog and reveals more periods of concentrated activity when compared to permanent network observations. The dense sampling also allows the ability to discriminate between different types of seismic signals including VT, LP, DLP, and surface sources, and to identify subgroups within the major groups (eg: low magnitude VT and hybrid LP). These results are likely not unique to Mount St. Helens but rather to the dense sampling afforded by the large-N array. The upper crustal LP earthquakes occurring between the main upper crustal magma chamber and the summit crater are important signals to continue monitoring, possibly through template detection using permanent network stations. An investigation into the source(s) causing LP seismicity is the next step in understanding their role in magmatic processes at Mount St. Helens.

References

Aizawa, K., Y. Ogawa, & T. Ishido (2009), Groundwater flow and hydrothermal systems within volcanic edifices: Delineation by electric self-potential and magnetotellurics, J. Geophys. Res., 114, B01208, doi:10.1029/2008JB005910.

Aso, N., & V. C. Tsai (2014), Cooling magma model for deep volcanic long-period earthquakes. J. Geophys. Res.-Sol. Earth 119, 8442–8456.

Bean, C. J., L. De Barros, I. Lokmer, J.-P. Metaxian, G. O'Brien, & S. Murphy (2014), Long-period seismicity in the shallow volcanic edifice formed from slow-rupture earthquakes, Nat. Geosci., 7(1), 71–75, doi:10.1038/ngeo2027.

Bedrosian, P. A., M. J. Unsworth, & M. J. S. Johnston (2007), Hydrother- mal circulation at Mount St. Helens determined by self-potential measurements, J. Volcanol. Geotherm. Res., 160, 137–146, doi:10.1016/ j.jvolgeores.2006.09.003.

Buurman, H., & M. E. West (2010), Seismic precursors to volcanic explosions during the 2006 eruption of Augustine Volcano, in The 2006 Eruption of Augustine Volcano, Alaska, U.S. Geol. Surv. Prof. Pap., 1769, edited by J. A. Power, M. L. Coombs, and J. T. Freymueller, chap. 2, pp. 41–57, U.S. Geological Survey, Reston, Va.

Christiansen, R.L., & D.W. Peterson (1981), The 1980 Eruptions of Mount St. Helens, Washington: Chronology of the 1980 eruptive activity, *U.S. Geological Survey Professional Paper*, 1250, 17-30.

Chouet, B. & B. R. Julian (1985), Dynamic of an expanding fluid-filled crack. J. Geophys. Res. 90, 11187–11198.

Chouet, B. A. (1992), in Volcanic Seismology (eds Gasparini, P., Scarpa, R. & Aki, K.) 133–156 (Springer).

Chouet, B., G. Saccorotti, M. Martini, P. Dawson, G. De Luca, G. Milana, & R. Scarpa (1997), Source and path effects in the wavefields of tremor and explosions at Stromboli Volcano, Italy, J. Geophys. Res., 102, 15,129–15,150.

Clynne, M. A., Calvert, A. T., Wolfe, E. W., Evarts, R. C., Fleck, R. J., & M. A. Lanphere (2008), The Pleistocene eruptive history of Mount St. Helens, Washington—from 300,000 to 12,800 years ago. In: Sherrod, D.R., Scott, W.E., Stauffer, P.H. (Eds.), A Volcano Rekindled: The Renewed Eruption of Mount St. Helens, 2004–2006. U.S. Geol. Surv., p. 1750.

Defant, M. J. & M. S. Drummond (1993), Mount St Helens: potential example of the partial melting of the subducted lithosphere in a volcanic arc. Geology 21, 547–550.

Denlinger, R. P., & S. C. Moran (2014), Volcanic tremor masks its seismogenic source: Results from a study of noneruptive tremor recorded at Mount St. Helens, Washington, J. Geophys. Res. Solid Earth, 119, 2230–2251, doi:10.1002/2013JB010698.

Freed, D. (2008), Cable-free nodes: The next generation land seismic system, Leading Edge, 27(7), 878–881. Gharti, H. N., V. Oye, M. Roth, and D. Kühn (2010), Automated

microearthquake location using envelope stacking and robust global optimization, Geophysics, 75(4), MA27–MA46.

Hansen, S. M. & B. Schmandt (2015), Automated detection and location of microseismicity at Mount St Helens with a large-N geophone array. Geophys. Res. Lett. 42, 7390–7397.

Hansen, S. M., Schmandt, B., Levander, A., Kiser, E., Vidale, J. E., Abers, G. A., & K. C. Kreager (2016), Seismic evidence for a cold serpentinized mantle wedge beneath Mount St Helens. Nat. Commun. 7, 13242 doi: 10.1038/ncomms13242.

Harjes, H.P., & M. Henger (1973), Array-Seismologie, Z. Geophs., 39, 865–905.

Harrington, R. M. & E. E. Brodsky (2007)., Volcanic hybrid earthquakes that are brittle-failure events. Geophys. Res. Lett. 34, L06308.

Iverson, R.M., D. Dzurisin, C.A. Gardner, T.M. Gerlach, R.G. LaHusen, M. Lisowski, J.J. Major, S.D. Malone, J.A. Messerich, S.C. Moran, J.S. Pallister, A.I. Qamar, S.P, Schilling, and J.W. Vallance (2006), Dynamics of seismogenic volcanic extrusion at Mount St. Helens in 2004-05, Nature, 444, 439-443. doi:10.1038/nature05322.

Kiser, E.,I. Palomeras, A. Levander, C. Zelt, S. Harder, B. Schmandt, S. Hansen, K. Creager, & C. Ulberg (2016), 3D Vp travel time tomography of the iMUSH active source seismic data, AGU Fall Meeting Abstracts, V43G-07.

La Rocca, M., & D. Galluzzo (2016), Volcanic tremor at Mt Vesuvius associated with low frequency shear failures, *Earth and Plan. Sci. Let., 442,* doi:hep://dx.doi.org/10.1016/j.epsl. 2016.02.048.

Matoza, R.S., Hedlin, M.A.H., & M.A. Garces (2007) An infrasound array study of Mt. St. Helens J. Volcanol. Geotherm. Res., 160 (2007), pp. 249–262, http://dx.doi.org/10.1016/j.jvolgeores.2006.10.006.

Matoza, R. S., P. M. Shearer, & P. G. Okubo (2014), High-precision relocation of long-period events beneath the summit region of Kīlauea Volcano, Hawaii, from 1986 to 2009, Geophys. Res. Lett., 41, 3413–3421, doi:10.1002/2014GL059819.

Matoza, R. S., B. A. Chouet, P. B. Dawson, P. M. Shearer, M. M. Haney, G. P. Waite, S. C. Moran, & T. D. Mikesell (2015), Source mechanism of small long-period events at Mount St. Helens in July 2005 using template matching, phase-weighted stacking, and full-waveform inversion, J. Geophys. Res. Solid Earth, 120, doi:10.1002/2015JB012279.

McNutt, S. R. (2005), Volcanic seismology. Annu. Rev. Earth Planet. Sci. 32, 461–491.

McCrory, P. A., J. L. Blair, D. H. Oppenheimer, & S. R. Walter (2004), Depth to the Juan de Fuca slab beneath the Cascadia subduction margin: A 3-D model for sorting earth-quakes, USGS DS-91, U. S. Geol. Surv., Reston, Va.

Meng, X., Hartog, J. R., Schmandt, B., Hotovec-Ellis, A. J., Hansen, S. M., Vidale, J. E., & J. Vanderplas (2016), Systematic detection of seismic events at Mount St. Helens with an ultra-dense array, AGU Fall Meeting Abstracts, V33E-3168.

Mills, H.H. (1991). Temporal Variation of Mass-Wasting Activity in Mount St. Helens Crater, Washington, USA - Indicated by Seismic Activity. Arctic and Alpine Research 23(4), 417-423.

Moran, S. C., Matoza R. S., Garces M. A., Hedlin M. A. H., Bowers D., Scot W. E., Sherrod D. R., & J. W. Wallace (2008), Seismic and acoustic recordings of an unusually large rockfall at Mount St. Helens, Washington, Geophys. Res. Lett. 35, L19302, doi:10.1029/2008GL035176.

Moran, S. C., S. D. Malone, A. I. Qamar, W. Thelen, A. K. Wright, & J. Caplan-Auerback (2008), 2004-2005 seismicity associated with the renewed dome-building eruption of Mount St. Helens, in A Volcano rekindled: the first year of renewed eruptions at Mount St. Helens, 2004-2006, edited by D. R. Sherrod, W. E. Scott, and P. H. Stauffer, U.S. Geolog. Surv. Prof. Pap., 1750.

Mullineaux, D. R. & Crandell, D. R. (1981), in The 1980 Eruptions of Mount St. Helens, Washington (eds Lipman, P. L. & Mullineaux, D. R.) 3–15 (USGS Professional Paper 1250, US Geological Survey, Washington DC).

Neuberg, J., Luckett, R., Baptie, V. & K. Olsen (2000), Models of tremor and low-frequency earthquake swarms on Montserrat. J. Volcanol. Geotherm. Res. 101, 83–104.

Neuberg, J., & T. Pointer (2000), Effects of volcano topography on seismic broad-band waveforms, Geophysics Journal International, 143, 239-248, doi: 10.1046/j.1365-246x.2000.00251.x.

Neuberg, J., Tuffen H., Collier L., Green D., Powell T., & D. Dingwell (2006), The trigger mechanism of low-frequency earthquakes on Montserrat, J. Volcanol. Geotherm. Res., 153, 37–50.

Nichols, M. L., Malone, S. D., Moran, S. C., Thelen, W. A. & J. E. Vidale (2011), Deep long-period earthquakes beneath Washington and Oregon volcanoes. J. Volcanol. Geotherm. Res. 200, 116–128.

Roman, D.C., 2005. Numerical models of volcanotectonic earthquake triggering on non-ideally oriented faults. Geophysical Research Letters 32, L02304. http://dx.doi.org/10.1029/2004GL021549.

Roman, D.C., & K.V. Cashman (2006), The origin of volcano-tectonic earthquake swarms. Geology 34 (6), 457–460.

Rost, S., & C. Thomas (2002), Array Seismology: Methods and applications, Rev. Geophys., 40, doi:10.1029/2000RG000100.

Rutherford, M.J., & P.M. Hill (1993), Magma ascent rates from amphibole breakdown: an experimental study applied to the 1980–1986 Mount St. Helens eruptions: J. of Geophys. Res., v. 98, no. B11, p. 19667–19685.

Scandone, R., & S.D. Malone (1985), Magma supply, magma discharge and readjustment of the feeding system of mount St. Helens during 1980: Journal of Volcanology and Geothermal Research, v. 23, p. 239–262, doi:10.1016/0377-0273(85)90036-8.

Shelly, D. R., G. C. Beroza, & S. Ide (2007), Non-volcanic tremor and low-frequency earthquake swarms, Nature, 446 (7133), 305–307.

Slater, D., & D. Hollis (2012), California's dense urban environment spawns friendlier 3D seismic survey design, Oil Gas J., 110(11), 54.

Thelen, W. A., K. Allstadt, S. De Angelis, S. D. Malone, S. C. Moran, & J. Vidale (2013), Shallow repeating seismic events under an alpine glacier at Mount Rainier, Washington, USA, J. Glaciol., 59(214), 345-356, doi:10.3189/2013JoG12J111.

Ukawa, M., & H. Tsukahara (1996), Earthquake swarms and dike intrusions off the east coast of Izu Peninsula, central Japan: Tectonophysics, v. 253, p. 285–303, doi: 10.1016/0040- 1951(95)00077-1.

Waite, G. P., B. A. Chouet, & P. B. Dawson (2008), Eruption dynamics at Mount St. Helens imaged from broadband seismic waveforms: Interaction of the shallow magmatic and hydrothermal systems, J. Geophys. Res., 113, B02305, doi:10.1029/2007JB005259.

Waite, G. P. & S. C. Moran (2009), VP Structure of Mount St Helens, Washington, USA, imaged with local earthquake tomography. J. Volcanol. Geotherm. Res. 182, 113–122.

Waldhauser F., & W. L. Ellsworth (2000), A double- difference earthquake location algorithm: Method and application to the northern Hayward fault, California. Bull. Seis. Soc. Am. 90:1353–68.

Wiemer, S., & S. R. McNutt (1997), Variations in the frequency-magnitude distribution with depth in two volcanic areas: Mount St. Helens, Washington, and Mt. Spurr, Alaska, Geophys. Res. Lett., 24(2), 189–192, doi:10.1029/96GL03779.